

NASA Technical Memorandum 107585

**Kinematics of an In-Parallel Actuated Manipulator
Based on the Stewart Platform Mechanism**

Robert L. Williams II

March 1992



**National Aeronautics and
Space Administration**

**Langley Research Center
Hampton, VA 23665**

KINEMATICS OF AN IN-PARALLEL ACTUATED MANIPULATOR BASED ON THE STEWART PLATFORM MECHANISM

Robert L. Williams II
NASA Langley Research Center

ABSTRACT

This paper presents kinematic equations and solutions for an in-parallel actuated robotic mechanism based on Stewart's platform. These equations are required for inverse position and resolved rate (inverse velocity) platform control. NASA Langley has a Vehicle Emulator System (VES) platform designed by M.I.T., which is based on Stewart's platform.

The inverse position solution is straight-forward and computationally inexpensive. Given the desired position and orientation of the moving platform with respect to the base, the lengths of the prismatic leg actuators are calculated.

The forward position solution is more complicated and theoretically has sixteen solutions. The position and orientation of the moving platform with respect to the base is calculated given the leg actuator lengths. Two methods are pursued in this paper to solve this problem. The first is based on a simplified model where the six moving platform ball joint locations are limited to three pairs. The second method accommodates the exact model. Both use numerical solution techniques; the first is a fixed-point iteration, while the second is a gradient-correction Newton-Raphson method. The simplified model results in error when applied to the VES model. A comparison of model error and computation time is presented, to contrast the two forward position methods.

The resolved rate (inverse velocity) solution is derived. Given the desired Cartesian velocity of the end-effector, the required leg actuator rates are calculated. The Newton-Raphson Jacobian matrix resulting from the second forward position kinematics solution is a modified inverse Jacobian matrix. This represents a significant computation savings when using resolved rate control and the second forward position method. No matrix inversion is required for the resolved rate solution, and thus this control method is free of singularities.

Examples and simulations are given for the VES. Translation and rotation motions are studied to demonstrate the leg inputs, the forward position solution convergence, and the simplified forward position model error for the platform under inverse position or resolved rate control.

1 INTRODUCTION

In-parallel actuated manipulators are robotic mechanisms with a closed-chain, parallel kinematic structure, as opposed to the open-chain, serial kinematic structure of common industrial manipulators. Although serial manipulators are more widely applied due in part to their anthropomorphic nature, interest in parallel manipulators is growing because of several advantages. Compared to serial manipulators, parallel manipulators have a higher structural stiffness, which eliminates the cantilever effect of open serial chains and allows greater positioning accuracy and repeatability. Associated with this is a greater capacity to withstand or apply external loads. The payload-to-weight ratio for parallel manipulators is significantly higher than for serial manipulators. Dynamic characteristics are improved due to less mass and base-mounted actuators, which allows higher operating speeds. The advantages of parallel manipulators are inherent in the mechanical structure, allowing less sophisticated controllers to achieve better performance, compared to serial manipulators. A major disadvantage of parallel manipulators is a reduced workspace. Serial manipulators generally have a larger overall workspace with the ability to reach into small spaces. Hunt (1983) provides a good introduction and overview of in-parallel actuated robotic mechanisms. A kinematic, dynamic, and workspace study of planar parallel robotic mechanisms is given in Williams (1988).

Stewart platform-based mechanisms are the most common practical implementation of in-parallel actuated manipulators to date. The Stewart platform was originally designed as an aircraft simulator (Stewart, 1965). The original Stewart's platform had three legs, each articulated with a revolute joint in the center. The parallel nature of a common Stewart platform adaptation is shown in the general kinematic diagram of Fig. 1. This device consists of a moving platform and a fixed base, each with six spherical joints. Connecting the platform and base are six legs with prismatic joints. The platform of Fig. 1 theoretically has twelve degrees of freedom, calculated by the Kutzbach equation, Eq.

1. (Mabie and Reinholtz, 1987). In Eq. 1, DOF is the number of degrees of freedom, N is the number of links, including the fixed link, and J_i is the number of i - degree of freedom joints in the manipulator. Prismatic joints have one and spherical joints three degrees of freedom.

$$\begin{aligned}
 DOF &= 6(N - 1) - 5J_1 - 4J_2 - 3J_3 - 2J_4 - J_5 \\
 DOF &= 6(14 - 1) - 5(6) - 3(12) \\
 DOF &= 12
 \end{aligned}
 \tag{1}$$

However, six of these twelve degrees of freedom are useless freedoms, rotations about the axes of each leg. Practical designs of such platforms constrain these six extra freedoms. The platform thus has six degrees of freedom which allow general positioning and orienting in three dimensions.

Most current Stewart platform applications are in aircraft simulators and related fields. Dieudonne, et. al., (1972) present the inverse and forward kinematics for a six degree of freedom aircraft motion platform simulator. These authors use the Newton-Rapshon method to solve the forward kinematics problem (referred to in their paper as the inverse transformation). Application to real-time computing is studied. In recent years, however, several authors have considered the six degree of freedom platform for robotic applications (e.g. Fichter (1986), Powell (1982), Sugimoto (1987), and Yang and Lee (1984)). These papers include theoretical modeling and practical implementation of Stewart platform-based manipulators and other in-parallel actuated manipulators.

There is an interesting duality concerning kinematic solutions of serial vs parallel manipulators. For serial manipulators, the forward position kinematics solution is generally straightforward and unique, and the inverse kinematics solution involves coupled nonlinear equations with multiple solutions. The opposite is generally true for in-parallel actuated manipulators (Williams, 1988). Analytical solutions of the forward position kinematics problem for parallel manipulators are cumbersome, when they exist. Analytical solutions

boil down to solving high-ordered polynomial equations which require numerical techniques when the order is greater than four. The platform equation is an even ordered sixteenth degree polynomial, which may be transformed into a general eighth order polynomial (Nanua, et. al., 1990). This polynomial involving grossly complicated terms is solved numerically, and the sixteen possible solutions are extracted. It is often more efficient to solve the basic kinematic equations numerically (Nguyen, et. al., 1991). This method returns one of the sixteen possible solutions which is nearest to the initial guess. The platform kinematics solutions of Nguyen, et. al. (1991) is similar to that of Dieudonne, et. al. (1972) A promising compromise is the method of homotopy (Watson, 1990). This is an efficient numerical technique for solving systems of nonlinear equations which requires no initial guess and returns all possible solutions. Homotopy is not pursued in the current paper.

This paper presents forward and inverse position kinematics, plus the resolved rate solution (inverse velocity kinematics) for the general Stewart platform based parallel manipulator in Fig. 1. The Vehicle Emulator System (VES), a platform to be used for studies of multiple manipulator dynamics and disturbance compensation, is used in computer simulations. The inverse position kinematics solution is presented first. This solution is unique, straight-forward, and computationally inexpensive. Two methods are then presented for the forward position kinematics solution. The first deals with a simplified platform model and is adapted from {Nanua, et. al., 1990}. The second is for the exact platform model and follows the method of {Nguyen, et. al., 1991}. Both models use a numerical technique to solve the basic coupled nonlinear forward position kinematics equations. The simplified model uses a one-point iteration method which is a divergence from Nanua, et. al. (1990), while the exact model uses a Newton-Raphson method with first order gradient correction. An advantage of the latter method is that the Newton-Raphson Jacobian matrix yields the platform inverse Jacobian matrix with little modification. Therefore, the resolved rate (inverse velocity) solution follows with little additional computation. Static examples are

given to demonstrate calculations for the equations of this paper. Platform simulations are presented to demonstrate translation and rotation motion. In addition, the simulations study the error resulting from the simplified forward kinematics model.

2 SYMBOLS

VES

$\{m\}$

$\{B\}$

$\{P\}$

$L_i, i = 1, 2, \dots, 6$

$\begin{bmatrix} n \\ m \\ T \end{bmatrix}$

$\begin{bmatrix} n \\ m \\ R \end{bmatrix}$

r_{ij}

$\{{}^n \mathbf{V}_m\}$

$\|\mathbf{V}\|$

$|\mathbf{A} \mathbf{B}|$

c_i, s_i, t_i

$\mathbf{B}_i, i = 1, 2, \dots, 6$

$\mathbf{P}_i, i = 1, 2, \dots, 6$

$\mathbf{Q}_i, i = 1, 2, 3$

$\{B_{ix}, B_{iy}, 0\}^T$

$\{P_{ix}, P_{iy}, 0\}^T$

$\{O_{ix}, O_{iy}, 0\}^T$

$a_i, i = 1, 2, 3$

$b_i, i = 1, 2, 3$

$\mathbf{O}_i, i = 1, 2, 3$

$r_i, i = 1, 2, 3$

$N_i, i = 1, 2, 3$

$\beta_i, i = 1, 2, 3$

$\theta_i, i = 1, 2, 3$

${}^B \mathbf{q}_i, i = 1, 2, 3$

$D_i, E_i, F_i, i = 1, 2, \dots, 5$

$\{Q\}$

$\hat{i}, \hat{j}, \hat{k}$

$\begin{bmatrix} B \\ P \\ T_s \end{bmatrix}$

E_T

E_R

$[R_E]$

r_B

r_P

$\{x, y, z\}^T$

$\theta_x, \theta_y, \theta_z$

\mathbf{X}

\dot{C}

$\dot{L}_i, i = 1, 2, \dots, 6$

$\{\dot{x}, \dot{y}, \dot{z}\}^T$

$\{\omega_x, \omega_y, \omega_z\}^T$

$\{\dot{\mathbf{X}}\}$

${}^B \{\dot{\mathbf{X}}\}$

${}^B [J]$

${}^B [J_M]$

$[J_{NR}]$

$\delta \mathbf{X}$

ϵ

Vehicle Emulator Simulator

Dextral Cartesian coordinate frame m

Fixed base coordinate frame

Moving platform coordinate frame

Variable platform leg lengths

Homogeneous transformation matrix of $\{m\}$ relative to $\{n\}$

Orthonormal rotation matrix of $\{m\}$ relative to $\{n\}$

Element (i,j) of $\begin{bmatrix} B \\ P \\ R \end{bmatrix}$

Position vector from origin of $\{n\}$ to $\{m\}$, expressed in $\{n\}$

Euclidean norm of \mathbf{V}

Distance between \mathbf{A} and \mathbf{B}

$\cos\theta_i, \sin\theta_i, \tan\theta_i$

Fixed base joint locations

Moving platform joint locations

Moving platform joint locations in simplified model

Components of ${}^B \mathbf{V}_{B_i}$

Components of ${}^P \mathbf{V}_{P_i}$

Components of ${}^B \mathbf{V}_{O_i}$

Fixed lengths between moving platform joints in simplified model

Fixed lengths between fixed base joints

Intersection of $|\mathbf{B}_{2i} \mathbf{B}_{2i-1}|$ and its normal to \mathbf{Q}_i in simplified model

Distance from \mathbf{B}_i to \mathbf{O}_i along $|\mathbf{B}_{2i} \mathbf{B}_{2i-1}|$ in simplified model

Length of normal to $|\mathbf{B}_{2i} \mathbf{B}_{2i-1}|$ from \mathbf{O}_i to \mathbf{Q}_i

Fixed angle from X_B to normal between $|\mathbf{B}_{2i} \mathbf{B}_{2i-1}|$ and origin of $\{B\}$

Angle variables from base to ${}^B \mathbf{q}_i$ in simplified model

Unit direction vectors in the direction of N_i , simplified model

Kinematic terms for simplified model

Intermediate frame for forward kinematics, simplified model

Columns of $\begin{bmatrix} B \\ Q \\ R \end{bmatrix}$

Simplified forward position kinematics solution, with error

Translational error in $\begin{bmatrix} B \\ P \\ T_s \end{bmatrix}$

Rotational error in $\begin{bmatrix} B \\ P \\ T_s \end{bmatrix}$

Rotational error difference matrix

Radius from origin of $\{B\}$ to any \mathbf{B}_i

Radius from origin of $\{P\}$ to any \mathbf{P}_i

Components of ${}^B \mathbf{V}_P$

Z - Y - X Euler angles describing $\begin{bmatrix} B \\ P \\ R \end{bmatrix}$

$\{x, y, z, \theta_x, \theta_y, \theta_z\}^T$

Time derivative of C

Linear velocity of variable leg lengths

Linear velocity of $\{P\}$ with respect to $\{B\}$, expressed in $\{B\}$

Angular velocity of $\{P\}$ with respect to $\{B\}$, expressed in $\{B\}$

$\{\dot{x}, \dot{y}, \dot{z}, \dot{\theta}_x, \dot{\theta}_y, \dot{\theta}_z\}^T$

$\{\dot{x}, \dot{y}, \dot{z}, \omega_x, \omega_y, \omega_z\}^T$, expressed in $\{B\}$

Jacobian matrix expressed in $\{B\}$, associated with ${}^B \{\dot{\mathbf{X}}\}$

Modified Jacobian matrix expressed in $\{B\}$, associated with $\{\dot{\mathbf{X}}\}$

Jacobian matrix for Newton-Raphson solution procedure

Correction vector for Newton-Raphson solution procedure

Tolerance for numerical method convergence

3 PHYSICAL DESCRIPTION OF THE VES

The Automation Technology Branch of NASA Langley Research Center plans to use a platform designed and built by M.I.T., named the Vehicle Emulator System (VES). This platform is an adaptation of Stewart's platform. The original Stewart's platform aircraft simulator had only three legs articulated with a middle revolute joint (Stewart, 1965). Multiple serial manipulators can be mounted on the platform for disturbance compensation experiments. The platform can represent a moving manipulator base in space, such as the Space Shuttle Remote Manipulator System (RMS) or a free-flying vehicle.

The VES platform kinematic diagram is shown in Fig. 2. There are six legs with hydraulically actuated prismatic joints. The total leg lengths are denoted $L_i, i = 1, 2, \dots, 6$. The minimum total leg length is 1.524 m(60 in) and the maximum is 2.286 m(90 in). The fixed base ball joint locations are $B_i, i = 1, 2, \dots, 6$ and the moving platform ball joint locations are $P_i, i = 1, 2, \dots, 6$. Figures 3a and b show the fixed base and moving platform geometry, respectively. The definitions for $\{B\}$ and $\{P\}$ are shown on these figures. As evident from Figs. 3a and b, there is symmetry in the design. Ball joint locations occur in pairs on both the fixed and moving platforms, each pair separated by 0.152 m(6 in). The base joints lie on a circle of radius $r_B = 1.340$ m(52.77 in) and the moving platform joints lie on a circle of radius $r_P = 0.305$ m(12.00 in). The components of vectors ${}^B \mathbf{V}_{B_i}$ and ${}^P \mathbf{V}_{P_i}$ are given in Appendix A. The homogeneous transformation matrix ${}^B_P T$ describes the position and orientation of $\{P\}$ relative to $\{B\}$ (Craig, 1988). Equation 2 gives the position and orientation decoupling of ${}^B_P T$.

$${}^B_P T = \left[\begin{array}{ccc|c} & & & \{^B \mathbf{V}_P\} \\ \hline & & & \\ \hline 0 & 0 & 0 & 1 \end{array} \right] \quad (2)$$

When all six leg lengths are equal, ${}^B_P R = [I]$, and ${}^B \mathbf{V}_P = \{0, 0, h\}^T$, where h is a displacement along Z_B .

4 POSITION KINEMATICS

The methods and equations of this paper are derived for the general platform of Fig. 1. The VES platform is used for examples and simulations.

Inverse Position Kinematics

The inverse position kinematics problem solves for the joint variables given the position and orientation of the moving platform with respect to the base: Find $L_i, i = 1, 2, \dots, 6$, given ${}^B_P T$. The solution is straight-forward and unique, based on the geometry of Fig. 1. Given ${}^B_P T$, the location of the moving platform in space is completely determined. The leg lengths are solved using the Euclidean norm between corresponding base and platform ball joint locations.

$$L_i = \| {}^B \mathbf{V}_{P_i} - {}^B \mathbf{V}_{B_i} \| \quad i = 1, 2, \dots, 6 \quad (3)$$

In order to express the moving platform ball joint locations in $\{B\}$, Eq. 4 is used.

$${}^B \mathbf{V}_{P_i} = [{}^B_P T]^P \mathbf{V}_{P_i} \quad (4)$$

Values for ${}^B \mathbf{V}_{B_i}$ and ${}^P \mathbf{V}_{P_i}$ are given in Appendix A, based on Figs. 3a and b.

The inverse position kinematics solution was used to find a minimum workspace for the VES platform. This workspace is the largest cubical volume reachable by the platform in translation, with ${}^B_P R = [I]$. The conservative minimum workspace is a cube of side $s = 0.457m(1.5ft)$, determined using trial and error subject to $L_{min} = 1.524m$ and $L_{max} = 2.286m$. For a more complete treatment of the platform workspace, refer to Cwiakala (1986).

Forward Position Kinematics

The forward position kinematics problem solves for the position and orientation of the moving platform with respect to the base given the joint variables: Find ${}^B_P T$, given $L_i, i = 1, 2, \dots, 6$. This problem involves coupled nonlinear equations. No analytical solution

exists because the reduced polynomial order of the problem is sixteen (Nanua, et. al., 1990). This means that potentially sixteen solutions exist. There are no analytical solutions to polynomial of order greater than four.

This section present two forward position kinematics solution methods. The first is derived from a simplified platform model, adapted from Nanua, et. al. (1990). Method two, based on Nguyen, et. al. (1991) involves the exact theoretical platform kinematic model. Both forward position solutions use an iterative method. The first is a fixed-point iteration method. The second method uses a first order Newton-Raphson gradient correction. The associated Jacobian matrix is shown to lead to the resolved rate solution in Section 4. The first method uses a simpler iteration, requiring less computation per cycle. The first method has inherent error because the moving platform ball joints are located in three pairs instead of the distinct locations in Fig. 2. The theoretical error associated with the second method is essentially zero, dependent on the convergence tolerance and the computer precision.

Simplified Model

Nanua, et. al. (1990) claim to present the first analytical forward position kinematics solution for a Stewart platform-based manipulator. Their work is based on a simplified model of Fig. 1. The joint locations B_i can occupy any position. However, the joint locations P_i are restricted as follows: P_1 and P_2 are co-located at Q_1 , P_3 and P_4 at Q_2 , and P_5 and P_6 at Q_3 . The simplified kinematic model for the VES platform is shown in Fig. 4a. Figure 4b presents the associated moving platform detail. The fixed base is unchanged, pictured in Fig. 3a.

The following fixed lengths are defined for the moving and fixed platforms, respectively.

$$\begin{aligned} a_1 &= |Q_1 Q_2| \\ a_2 &= |Q_2 Q_3| \\ a_3 &= |Q_3 Q_1| \end{aligned} \tag{5a}$$

$$\begin{aligned}
b_1 &= |\mathbf{B}_1\mathbf{B}_2| \\
b_2 &= |\mathbf{B}_3\mathbf{B}_4| \\
b_3 &= |\mathbf{B}_5\mathbf{B}_6|
\end{aligned} \tag{5b}$$

Three kinematic chains are studied in the simplified model: $\mathbf{B}_1\mathbf{Q}_1\mathbf{B}_2\mathbf{B}_1$, $\mathbf{B}_3\mathbf{Q}_2\mathbf{B}_4\mathbf{B}_3$, and $\mathbf{B}_5\mathbf{Q}_3\mathbf{B}_6\mathbf{B}_5$. A representative chain is shown in Fig. 5 where $i = 1, 2, 3$ for the three chains. Point \mathbf{O}_i is the intersection between $|\mathbf{B}_{2i}\mathbf{B}_{2i-1}|$ and its normal to \mathbf{Q}_i . As the input leg lengths vary, the locations of \mathbf{Q}_i and \mathbf{O}_i move, the unit direction vector ${}^B\mathbf{q}_i$ changes, and the lengths r_i and N_i change. The cosine law is applied to determine r_i from known information at each time step.

$$L_{2i}^2 = L_{2i-1}^2 + b_i^2 - 2L_{2i-1}b_i\cos\psi_i \tag{6}$$

$$r_i = L_{2i-1}\cos\psi_i \tag{7}$$

$$r_i = \frac{b_i^2 + L_{2i-1}^2 - L_{2i}^2}{2b_i} \tag{8}$$

The instantaneous value of N_i is determined via the Pythagorean theorem.

$$N_i = \sqrt{L_{2i-1}^2 - r_i^2} \tag{9}$$

With this information, a reduced simplified model is constructed as shown in Fig. 6. The forward position kinematic equations are derived from the following constraints, which dictate that the lengths between the moving platform joints remain constant.

$$\begin{aligned}
a_1^2 &= \|\mathbf{}^B\mathbf{V}_{Q1} - \mathbf{}^B\mathbf{V}_{Q2}\|^2 \\
a_2^2 &= \|\mathbf{}^B\mathbf{V}_{Q2} - \mathbf{}^B\mathbf{V}_{Q3}\|^2 \\
a_3^2 &= \|\mathbf{}^B\mathbf{V}_{Q3} - \mathbf{}^B\mathbf{V}_{Q1}\|^2
\end{aligned} \tag{10}$$

The left hand sides of Eq. 10 are known constants, given in Appendix A for the VES platform. The right hand sides are expressed through the platform geometry, with unknowns θ_i in terms ${}^B\mathbf{q}_i, i = 1, 2, 3$.

$${}^B\mathbf{V}_{Q_i} = \mathbf{}^B\mathbf{V}_{O_i} + N_i\mathbf{}^B\mathbf{q}_i \tag{11}$$

where:

$${}^B \mathbf{V}_{O_i} = {}^B \mathbf{V}_{B_{2i-i}} + \frac{r_i}{b_i} ({}^B \mathbf{V}_{B_{2i}} - {}^B \mathbf{V}_{B_{2i-i}}) = \begin{Bmatrix} O_{ix} \\ O_{iy} \\ 0 \end{Bmatrix} \quad (12)$$

The unit direction vectors ${}^B \mathbf{q}_i$, pointing from O_i to Q_i , are calculated using simple rotation matrices. The fixed angles β_i (pictured in Fig. 7) are measured in the fixed base plane from X_D to the normal between $|\mathbf{B}_{2i}\mathbf{B}_{2i-1}|$ and the origin of $\{B\}$.

$${}^B \mathbf{q}_i = \begin{Bmatrix} c\beta_i c_i \\ s\beta_i c_i \\ s_i \end{Bmatrix} \quad (13)$$

The forward position kinematics equations, Eqs. 14, 15, and 16, are obtained by substituting Eq. 11 into Eq. 10 and simplifying. First, Eqs. 12 and 13 are substituted into Eq. 11. Equations 14, 15, and 16 are three coupled transcendental equations in the three unknowns θ_1, θ_2 , and θ_3 .

$$D_1 c_1 + D_2 c_2 + D_3 c_1 c_2 + D_4 s_1 s_2 + D_5 = 0 \quad (14)$$

$$E_1 c_2 + E_2 c_3 + E_3 c_2 c_3 + E_4 s_2 s_3 + E_5 = 0 \quad (15)$$

$$F_1 c_3 + F_2 c_1 + F_3 c_3 c_1 + F_4 s_3 s_1 + F_5 = 0 \quad (16)$$

The coefficients for Eqs. 14, 15, and 16 are given below.

$$\begin{aligned} D_1 &= 2N_1 [c\beta_1(O_{1X} - O_{2X}) + s\beta_1(O_{1Y} - O_{2Y})] \\ D_2 &= -2N_2 [c\beta_2(O_{1X} - O_{2X}) + s\beta_2(O_{1Y} - O_{2Y})] \\ D_3 &= -2N_1 N_2 c(\beta_1 - \beta_2) \\ D_4 &= -2N_1 N_2 \\ D_5 &= (O_{1X} - O_{2X})^2 + (O_{1Y} - O_{2Y})^2 + N_1^2 + N_2^2 - a_1^2 \end{aligned} \quad (17)$$

$$\begin{aligned} E_1 &= 2N_2 [c\beta_2(O_{2X} - O_{3X}) + s\beta_2(O_{2Y} - O_{3Y})] \\ E_2 &= -2N_3 [c\beta_3(O_{2X} - O_{3X}) + s\beta_3(O_{2Y} - O_{3Y})] \\ E_3 &= -2N_2 N_3 c(\beta_2 - \beta_3) \\ E_4 &= -2N_2 N_3 \\ E_5 &= (O_{2X} - O_{3X})^2 + (O_{2Y} - O_{3Y})^2 + N_2^2 + N_3^2 - a_2^2 \end{aligned} \quad (18)$$

$$\begin{aligned} F_1 &= 2N_3 [c\beta_3(O_{3X} - O_{1X}) + s\beta_3(O_{3Y} - O_{1Y})] \\ F_2 &= -2N_1 [c\beta_1(O_{3X} - O_{1X}) + s\beta_1(O_{3Y} - O_{1Y})] \\ F_3 &= -2N_3 N_1 c(\beta_3 - \beta_1) \\ F_4 &= -2N_3 N_1 \\ F_5 &= (O_{3X} - O_{1X})^2 + (O_{3Y} - O_{1Y})^2 + N_3^2 + N_1^2 - a_3^2 \end{aligned} \quad (19)$$

At this point, Nanua, et. al. (1990) apply Bezout's method (Salmon, 1964) to Eqs. 14, 15, and 16 twice, eliminating θ_2 and θ_3 to solve for θ_1 "analytically". The two remaining unknowns are solved after θ_1 is known, using the tangent half-angle substitution (Williams, 1990) in Eqs. 14 and 16. The θ_1 solution is not truly analytical because it is calculated from a sixteenth order polynomial in the tangent half-angle of θ_1 , which must be solved using a numerical technique. The intermediate terms for the polynomial coefficients are not reported in Nanua, et. al. (1990). Upon determination of these coefficients using a computer symbolic manipulation program, these intermediate terms were found to be quite complex. Therefore, an alternate approach, an efficient Newton-Raphson iterative technique, was used to solve Eqs. 14, 15, and 16 directly for the three unknowns. This method is presented in Appendix B.

When the three unknown angles θ_i are solved, the simplified model approximation to ${}^B_P T$, ${}^B_P T_s$, is calculated with Eq. 20. The intermediate frame $\{Q\}$ is used (see Fig. 4b). Unit vectors $(\hat{i}, \hat{j}, \hat{k})$ are the columns of ${}^B_Q R$. The term ${}^B \mathbf{V}_{Q1}$ is determined from Eq. 11, using Eqs. 12 and 13.

$${}^B_P T_s = {}^B_Q T \left[{}^Q_P T \right] \quad (20)$$

$${}^B_Q T = \left[\begin{array}{ccc|c} \frac{{}^B_Q R}{} & & & \{ {}^B \mathbf{V}_Q \} \\ \hline 0 & 0 & 0 & 1 \end{array} \right] = \left[\begin{array}{ccc|c} \hat{i} & \hat{j} & \hat{k} & \{ {}^B \mathbf{V}_{Q1} \} \\ \hline 0 & 0 & 0 & 1 \end{array} \right] \quad (21)$$

$$\hat{i} = \frac{{}^B \mathbf{V}_{Q1} - {}^B \mathbf{V}_{Q2}}{\| {}^B \mathbf{V}_{Q1} - {}^B \mathbf{V}_{Q2} \|} \quad (21a)$$

$$\hat{j} = \frac{({}^B \mathbf{V}_{Q1} - {}^B \mathbf{V}_{Q2}) \times ({}^B \mathbf{V}_{Q2} - {}^B \mathbf{V}_{Q3})}{\| ({}^B \mathbf{V}_{Q1} - {}^B \mathbf{V}_{Q2}) \times ({}^B \mathbf{V}_{Q2} - {}^B \mathbf{V}_{Q3}) \|} \quad (21b)$$

$$\hat{k} = \frac{({}^B \mathbf{V}_{Q1} - {}^B \mathbf{V}_{Q2}) \times [({}^B \mathbf{V}_{Q1} - {}^B \mathbf{V}_{Q2}) \times ({}^B \mathbf{V}_{Q2} - {}^B \mathbf{V}_{Q3})]}{\| ({}^B \mathbf{V}_{Q1} - {}^B \mathbf{V}_{Q2}) \times [({}^B \mathbf{V}_{Q1} - {}^B \mathbf{V}_{Q2}) \times ({}^B \mathbf{V}_{Q2} - {}^B \mathbf{V}_{Q3})] \|} \quad (21c)$$

$${}^Q_R T = \begin{bmatrix} \frac{\sqrt{3}}{2} & \frac{1}{2} & 0 & -12\frac{\sqrt{3}}{2} \\ 0 & 0 & 1 & 0 \\ \frac{1}{2} & -\frac{\sqrt{3}}{2} & 0 & 6 \\ 0 & 0 & 0 & 1 \end{bmatrix} \quad (22)$$

The forward position kinematics solution ${}^B_P T_s$ from the simplified platform model has inherent error due to the simplified moving platform ball joint locations. (compare Figs. 3b and 4b). The simplified model was pursued because the solution algorithm was expected to be faster than the exact model. A measure of error is required to determine the deviation of the simplified model from the true solution. The error measure used is given in terms of translational error and rotational error. Let ${}^B_P T$ represent the true solution and ${}^B_P T_s$ the simplified model result.

The translational error is the Euclidean norm of the algebraic difference of the two position vectors.

$$E_T = \| {}^B \mathbf{V}_P - {}^B \mathbf{V}_{P_s} \| \quad (23)$$

The rotational error is more complicated because algebraic subtraction does not apply to rotation matrices. The following difference matrix is used.

$$[R_E] = [{}^B_P R_s]^{-1} [{}^B_P R] = [{}^B_P R_s]^T [{}^B_P R] \quad (24)$$

If there is no rotational error, $[R_E] = [I]$. A measure of rotational error is obtained by extracting the Z-Y-X Euler angles from $[R_E]$ (Craig, 1988). Denoting these as $\theta_E = \{\theta_{XE}, \theta_{YE}, \theta_{ZE}\}^T$, a single rotational error is obtained by using the Euclidean norm. If there is no rotational error, $\theta_E = \{0, 0, 0\}^T$.

$$E_R = \|\theta_E\| \quad (25)$$

The simplified model error is studied in a static example (Section 5) and in platform simulations (Section 6).

Exact Model

Nguyen, et. al. (1991) present an iterative forward position kinematics solution for a general platform, shown in Fig. 1. This method is attractive because it yields the exact theoretical solution, within the convergence tolerance. In addition, a modified inverse Jacobian matrix is extracted from the Newton-Raphson Jacobian matrix. Therefore, the resolved rate solution is achieved with little additional computational cost. The exact model for the VES platform is given in Fig. 2. Associated ball joint location details are shown in Fig. 3, and the corresponding vector components are presented in Appendix A. The forward position solution presented in this section is adapted from Nguyen, et. al. (1991).

Given the six actuator leg lengths, the forward position problem is to find ${}^B_P T$. The position and orientation structure of this homogeneous transformation matrix is given in Eq. 2. There are six unknowns associated with ${}^B_P T$, represented as $\mathbf{X} = \{x, y, z, \theta_x, \theta_y, \theta_z\}^T$. The position vector is:

$${}^B \mathbf{V}_P = \begin{Bmatrix} x \\ y \\ z \end{Bmatrix} \quad (26)$$

The Z-Y-X Euler convention (Craig, 1988) is chosen to represent the orientation of $\{P\}$ with respect to $\{B\}$, which leads to the following rotation matrix.

$${}^B_P R = \begin{bmatrix} r_{11} & r_{12} & r_{13} \\ r_{21} & r_{22} & r_{23} \\ r_{31} & r_{32} & r_{33} \end{bmatrix} = \begin{bmatrix} c_y c_z & -c_x s_z + s_x s_y c_z & s_x s_z + c_x s_y c_z \\ c_y s_z & c_x c_z + s_x s_y s_z & -s_x c_z + c_x s_y s_z \\ -s_y & s_x c_y & c_x c_y \end{bmatrix} \quad (27)$$

To derive the forward position kinematics equations, a vector loop closure equation is written for each leg, expressed in terms of the unknowns. Figure 8 shows the vector diagram for the i th actuator leg. This kinematic diagram includes the base and moving platform ball joint locations, plus $\{B\}$ and $\{P\}$. For $i = 1, 2, \dots, 6$, ${}^B_{B_i} R = [I]$; therefore, vectors expressed in $\{B_i\}$ have the same components as those in $\{B\}$. From Fig. 8, the vector loop closure equation is Eq. 28.

$${}^{B_i} \mathbf{V}_{P_i} = {}^{B_i} \mathbf{V}_P + {}^B_{B_i} R^T \mathbf{V}_{P_i} \quad (28)$$

where:

$${}^{B_i} \mathbf{V}_P = {}^B \mathbf{V}_P - {}^B \mathbf{V}_{B_i} \quad (29)$$

Let the moving platform and base spherical joint locations be denoted as follows.

$${}^P \mathbf{V}_{P_i} = \begin{Bmatrix} P_{ix} \\ P_{iy} \\ 0 \end{Bmatrix} \quad {}^B \mathbf{V}_{B_i} = \begin{Bmatrix} B_{ix} \\ B_{iy} \\ 0 \end{Bmatrix} \quad (30)$$

Using Eqs. 26, 27, 29, and 30 in Eq. 28, the vector representing leg i is Eq. 31. The orientation unknowns appear in the r_{ij} terms.

$${}^{B_i} \mathbf{V}_{P_i} = \begin{Bmatrix} x + r_{11}P_{ix} + r_{12}P_{iy} - B_{ix} \\ y + r_{21}P_{ix} + r_{22}P_{iy} - B_{iy} \\ z + r_{31}P_{ix} + r_{32}P_{iy} \end{Bmatrix} \quad (31)$$

The constraint equation for the i th leg is the Euclidean norm of the leg length.

$$L_i^2 = \|{}^{B_i} \mathbf{V}_{P_i}\|^2 \quad (32)$$

Substituting Eq. 28 into Eq. 32, the i th constraint equation is:

$$f_i(\mathbf{X}) = 0; \quad i = 1, 2, \dots, 6 \quad (33)$$

$$\begin{aligned} f_i(\mathbf{X}) = & x^2 + y^2 + z^2 + 2(P_{ix}r_{11} + P_{iy}r_{12})(x - B_{ix}) + 2(P_{ix}r_{21} + P_{iy}r_{22})(y - B_{iy}) + \\ & 2(P_{ix}r_{31} + P_{iy}r_{32})z - 2(xB_{ix} + yB_{iy}) + r_P^2 + r_B^2 - L_i^2 = 0 \end{aligned} \quad (34)$$

The unknowns $\theta_x, \theta_y, \theta_z$ appear in Eq. 34 through the r_{ij} terms, given in Eq. 27. The result reported in Eq. 34 was simplified using the following relationships. The first three are orthonormal constraints on rotation matrices. The values for r_B and r_P , given in Appendix A, are constant for all i .

$$r_{11}^2 + r_{21}^2 + r_{31}^2 = 1 \quad (35a)$$

$$r_{12}^2 + r_{22}^2 + r_{32}^2 = 1 \quad (35b)$$

$$r_{11}r_{12} + r_{21}r_{22} + r_{31}r_{32} = 0 \quad (35c)$$

$$r_B^2 = B_{ix}^2 + B_{iy}^2 \quad (35d)$$

$$r_P^2 = P_{ix}^2 + P_{iy}^2 \quad (35e)$$

Equation 34 is written for each of the six legs. The form of each equation is identical; the components of ${}^B\mathbf{V}_{B_i}$ and ${}^P\mathbf{V}_{P_i}$ change. Equation 34 can also be used for the inverse position kinematics solution. Given ${}^B_P\mathbf{T}$, $L_i, i = 1, 2, \dots, 6$ is easily calculated. The result is the same as that presented in Section 3.1.

To solve the forward position kinematics problem, the system is six coupled nonlinear equations in the six unknowns $\mathbf{X} = \{x, y, z, \theta_x, \theta_y, \theta_z\}^T$. The solution method is a first derivative gradient correction Newton-Raphson iterative technique. It is presented in Appendix C. When the solution is obtained to the desired convergence tolerance, ${}^B_P\mathbf{T}$ is formed using Eqs. 26 and 27 in Eq. 2.

5 VELOCITY KINEMATICS

Velocity kinematics is concerned with the relationship between the moving platform Cartesian velocities and the linear rates of change of the leg actuators. The forward velocity kinematics problem calculates the Cartesian velocities given the leg rates. The inverse velocity kinematics solution (resolved rate solution) solves for the leg rates given the Cartesian velocities.

The forward velocity equation is Eq. 36. The Jacobian matrix ${}^B[J]$ is a linear operator which maps actuator velocities into Cartesian velocities.

$${}^B\{\dot{\mathbf{X}}\} = {}^B[J] \{\dot{\mathbf{L}}\} \quad (36)$$

where:

$${}^B\{\dot{\mathbf{X}}\} = \{\dot{x}, \dot{y}, \dot{z}, \omega_X, \omega_Y, \omega_Z\}^T$$

$$\{\dot{\mathbf{L}}\} = \{\dot{L}_1, \dot{L}_2, \dots, \dot{L}_6\}^T$$

A common method for manipulator control is the resolved rate solution, obtained by inverting Eq. 36.

$$\{\dot{\mathbf{L}}\} = {}^B[J]^{-1} {}^B\{\dot{\mathbf{X}}\} \quad (37)$$

As mentioned previously, a modified inverse Jacobian matrix is extracted from the Newton-Raphson method Jacobian, associated with the exact forward position kinematics solution, given in Appendix C. This section presents the derivation of the modified inverse Jacobian matrix. The relationship between the modified inverse Jacobian matrix and that of Eq. 37 is also developed.

Moving the L_i^2 term to the right hand side of Eq. 34 and taking one time derivative yields Eq. 38.

$$2L_i \dot{L}_i = \sum_{j=1}^6 \frac{\partial f_i}{\partial X_j} \{\dot{X}_j\} \quad (38)$$

Dividing by $2L_i$, an equation similar to the form of Eq. 37 is obtained.

$$\dot{L}_i = \frac{1}{2L_i} \sum_{j=1}^6 \frac{\partial f_i}{\partial X_j} \{\dot{X}_j\} \quad (39)$$

The form of Eq. 39 differs from that of the resolved rate solution, Eq. 37, because

$${}^B\{\dot{\mathbf{X}}\} \neq \frac{d}{dt}\mathbf{X}. \quad (40)$$

In the above equation, equality holds for the translational velocities, but not the rotational velocities. The Cartesian translational velocities, plus the Z-Y-X Euler angle rates are defined to be:

$$\{\dot{\mathbf{X}}\} = \frac{d}{dt}\mathbf{X} = \{\dot{x}, \dot{y}, \dot{z}, \dot{\theta}_X, \dot{\theta}_Y, \dot{\theta}_Z\}^T \quad (41)$$

Therefore, the inverse Jacobian matrix in Eq. 39 is a modified inverse Jacobian matrix. From Appendix C, the modified inverse Jacobian matrix is related to the Newton-Raphson Jacobian matrix, as shown in Eq. 43. This result is intuitive because the inverse velocity problem and forward position iteration require the partial derivatives of the functions, Eq. 34, with respect to the Cartesian position variables, \mathbf{X} .

$$\{\dot{\mathbf{L}}\} = {}^B [J_M]^{-1} \{\dot{\mathbf{X}}\} \quad (42)$$

$${}^B [J_M]^{-1} = \left[\frac{1}{2L_i} \frac{\partial f_i}{\partial X_j} \right] = \left[\frac{1}{2L_i} J_{NR} \right] \quad (43)$$

To calculate the modified inverse Jacobian matrix, each component in all rows i of $[J_{NR}]$ is divided by $2L_i$. It is more efficient to factor this term out and divide only once per row. The terms of $[J_{NR}]$ are given in Appendix C.

The relationship between the modified and actual inverse Jacobian matrices is now presented. As noted previously, the Cartesian angular velocity vector is not obtained by time differentiation of the Euler angles. Rather, the following rotational velocity kinematic transformation is required (Kane, et. al. (1983), Appendix II).

$$\{\dot{\theta}\} = [A]\{\omega\} \quad (44)$$

$$\begin{Bmatrix} \dot{\theta}_X \\ \dot{\theta}_Y \\ \dot{\theta}_Z \end{Bmatrix} = \begin{bmatrix} 1 & s_x t_y & c_x t_y \\ 0 & c_x & -s_x \\ 0 & \frac{s_x}{c_y} & \frac{c_x}{c_y} \end{bmatrix} \begin{Bmatrix} \omega_X \\ \omega_Y \\ \omega_Z \end{Bmatrix}$$

With the definition in Eq. 41, the relationship between the modified and actual inverse Jacobian matrices is Eq. 46. This was obtained by using Eqs. 37, 42, and 44.

$${}^B[J_M]^{-1} = \begin{bmatrix} [J_{UL}] & | & [J_{UR}] \\ \hline [J_{LL}] & | & [J_{LR}] \end{bmatrix} \quad (45)$$

$${}^B[J]^{-1} = \begin{bmatrix} [J_{UL}] & | & [J_{UR}][A] \\ \hline [J_{LL}] & | & [J_{LR}][A] \end{bmatrix} \quad (46)$$

The resolved rate solution is Eq. 37, using Eq. 46. This paper does not present the symbolic form of Eq. 46. Rather, the resolved rate solution is obtained by using Eq. 44 and then Eqs. 41 and 45 substituted into Eq. 42.

As seen from Eqs. 37, 43, and 46, the resolved rate solution does not require a matrix inversion. Rather, the inverse platform Jacobian matrix is adapted from J_{NR} , given in Appendix C, Eqs. C.6. Equation 43 reveals that ${}^B[J_M]^{-1}$ always exists uniquely unless one or more $L_i = 0$, which is physically impossible. Therefore, the resolved rate solution is singularity-free. In contrast, many serial industrial manipulators have singularities which degrade overall performance.

Fichter (1986) found that singularities for a Stewart Platform-based manipulator are positions where the end-effector gains one or more degrees of freedom. This is in contrast to serial manipulator singularities where the manipulator loses one or more freedoms. However, this result was shown for the simplified platform model of Fig. 4a. The VES Platform model, Fig. 2, cannot be placed in the special configurations Fichter identified because the moving platform ball joints are separated by a finite distance. Therefore, uncontrollable added-freedom singularities do not occur in the VES Platform.

6 EXAMPLES

This section presents static examples to demonstrate computation for the kinematic equations of this paper applied to the VES platform. The first examples find ${}^B_P T$ for the minimum, middle, and maximum leg lengths, $L_{MIN} = 1.524$, $L_{MID} = 1.905$, and $L_{MAX} = 2.286$. The exact forward position kinematics solution (Section 3.2.2 and Appendix C) is used. At the minimum and maximum conditions, the workspace shrinks to a point. Example 1b is a good reset position for the VES platform, where $\mathbf{X} = \{0, 0, 1.531, 0, 0, 0\}^T$. The middle condition is defined as the average of the minimum and maximum leg lengths. Note that this does not exactly correspond to the average of the minimum and maximum Cartesian space values. Figure 9 shows the Z components of ${}^B \mathbf{V}_P$ as a function of $L_i, i = 1, 2, \dots, 6$ where all leg lengths are equal. This relationship is weakly non-linear, as seen by comparison with the dotted line in Fig. 9.

$$1a) \{L_{MIN}\} = \{1.524, 1.524, 1.524, 1.524, 1.524, 1.524\}^T$$

$${}^B_P T = \begin{bmatrix} 1.000 & 0.000 & 0.000 & 0.000 \\ 0.000 & 1.000 & 0.000 & 0.000 \\ 0.000 & 0.000 & 1.000 & 1.019 \\ 0 & 0 & 0 & 1 \end{bmatrix}$$

$$1b) \{L_{MID}\} = \{1.905, 1.905, 1.905, 1.905, 1.905, 1.905\}^T$$

$${}^B_P T = \begin{bmatrix} 1.000 & 0.000 & 0.000 & 0.000 \\ 0.000 & 1.000 & 0.000 & 0.000 \\ 0.000 & 0.000 & 1.000 & 1.531 \\ 0 & 0 & 0 & 1 \end{bmatrix}$$

$$1c) \{L_{MAX}\} = \{2.286, 2.286, 2.286, 2.286, 2.286, 2.286\}^T$$

$${}^B_P T = \begin{bmatrix} 1.000 & 0.000 & 0.000 & 0.000 \\ 0.000 & 1.000 & 0.000 & 0.000 \\ 0.000 & 0.000 & 1.000 & 1.985 \\ 0 & 0 & 0 & 1 \end{bmatrix}$$

A general input $\{\mathbf{X}\}$ is commanded for Example 2.

$$2) \{\mathbf{X}\} = \{0.200, 0.400, 1.500, 25.0, 15.0, 40.0\}^T$$

The transformation matrix ${}^B_P T$ is calculated using Eqs. 26 and 27 in Eq. 2.

$${}^B_P T = \begin{bmatrix} 0.740 & -0.499 & 0.451 & 0.200 \\ 0.621 & 0.764 & -0.173 & 0.400 \\ -0.259 & 0.408 & 0.875 & 1.500 \\ 0 & 0 & 0 & 1 \end{bmatrix}$$

From ${}^B_P T$, the inverse position kinematics solution is found with Eqs. 3 and 4.

$$\{\mathbf{L}\} = \{1.981, 1.828, 1.939, 2.143, 2.212, 1.672\}^T$$

Using these actuator leg lengths, both forward kinematics solutions are employed to reproduce the original ${}^B_P T$. For both methods, the convergence tolerance is $\epsilon = 0.000001$; the meaning is not the same for the two models (see Appendices B and C). In addition, the number of iterations to convergence and the error is presented for each method. The initial guess for each model is the nominal reset position, $\theta_i (i = 1, 2, 3) = \{73.8^\circ, 73.8^\circ, 73.8^\circ\}^T$ for the simplified model and $\mathbf{X} = \{0, 0, 1.531, 0, 0, 0\}^T$ for the exact model.

The simplified model (Section 3.2.1 and Appendix B) calculated the following ${}^B_P T_s$ in 19 iterations. The translational error is $E_T = 0.067m$. The rotation error difference matrix is given, extracting $\theta_{XE} = 6.144^\circ, \theta_{YE} = 5.387^\circ, \theta_{ZE} = 8.829^\circ$ and thus $E_R = 12.030^\circ$.

$${}^B_P T_s = \begin{bmatrix} 0.848 & -0.419 & 0.324 & 0.197 \\ 0.483 & 0.863 & -0.148 & 0.333 \\ -0.218 & 0.282 & 0.934 & 1.493 \\ 0 & 0 & 0 & 1 \end{bmatrix}$$

$$[R_E] = \begin{bmatrix} 0.984 & -0.143 & 0.108 \\ 0.153 & 0.984 & -0.092 \\ -0.094 & 0.107 & 0.989 \end{bmatrix}$$

The exact model (Section 3.2.2 and Appendix C) calculated the following ${}^B_P T$ in 6 iterations. The translational error is zero, to three decimal places. The rotation error difference matrix is given, extracting $\theta_{XE} = 0.083^\circ, \theta_{YE} = 0.040^\circ, \theta_{ZE} = -0.020^\circ$ and thus $E_R = 0.094^\circ$.

$${}^B_P T = \begin{bmatrix} 0.740 & -0.500 & 0.450 & 0.200 \\ 0.621 & 0.765 & -0.172 & 0.400 \\ -0.258 & 0.407 & 0.876 & 1.500 \\ 0 & 0 & 0 & 1 \end{bmatrix}$$

$$[R_E] = \begin{bmatrix} 1.000 & 0.000 & 0.001 \\ 0.000 & 1.000 & -0.002 \\ -0.001 & 0.001 & 0.999 \end{bmatrix}$$

7 PLATFORM SIMULATIONS

A series of three platform motion simulations is presented in this section. The first is a pure straight-line translation, the second is a pure rotational move, and the third is a combination of the first two. Smooth trajectory generation is ignored for these kinematic simulations.

For each simulation, the following steps are followed. The input is $\{\dot{\mathbf{X}}\}$, from which a series of eleven commanded homogeneous transformation matrices are obtained for each second, starting at zero and ending at ten seconds. Below, only the first and last of these are reported for each case. From this data, the inverse position kinematics problem is solved. With the inverse position solution as input, the simplified and exact forward position kinematics solutions are calculated for each second and compared to the original homogeneous transformation matrices. The error is calculated for the simplified model solution. The exact model solution error is zero, to the nearest thousandth place in the resulting homogeneous transformation matrices. The resolved rate solution is obtained with few calculations following the exact forward position solution. Each forward position simulation starts at the first computation step using the respective nominal reset positions given in Section 5 as an initial guess. The current solution is used as the initial guess for the remaining steps. The convergence tolerance is $\epsilon = 0.001$.

The input information is given below for each of the three simulations. The simulation results for the inverse position solutions are given in Figs. 10a, 11a, and 12a, for the translation, rotation, and translation/rotation simulations, respectively. The associated resolved rate solutions are given in Figs. 10b, 11b, and 12b. The simplified forward position solution errors are reported in Figs. 10c, 11c, and 12c.

1) Straight-Line Translation

$$\begin{Bmatrix} \dot{x} \\ \dot{y} \\ \dot{z} \end{Bmatrix} = \begin{Bmatrix} -0.005 \\ 0.030 \\ 0.060 \end{Bmatrix} \qquad \begin{Bmatrix} \dot{\theta}_x \\ \dot{\theta}_y \\ \dot{\theta}_z \end{Bmatrix} = \begin{Bmatrix} 0.0 \\ 0.0 \\ 0.0 \end{Bmatrix}$$

$$[{}^B_F T] = \begin{bmatrix} 1.000 & 0.000 & 0.000 & 0.000 \\ 0.000 & 1.000 & 0.000 & 0.000 \\ 0.000 & 0.000 & 1.000 & 1.100 \\ 0 & 0 & 0 & 1 \end{bmatrix}, \begin{bmatrix} 1.000 & 0.000 & 0.000 & -0.050 \\ 0.000 & 1.000 & 0.000 & 0.300 \\ 0.000 & 0.000 & 1.000 & 1.700 \\ 0 & 0 & 0 & 1 \end{bmatrix}$$

2) Pure Rotation

$$\begin{bmatrix} \dot{x} \\ \dot{y} \\ \dot{z} \end{bmatrix} = \begin{bmatrix} 0.0 \\ 0.0 \\ 0.0 \end{bmatrix} \quad \begin{bmatrix} \dot{\theta}_X \\ \dot{\theta}_Y \\ \dot{\theta}_Z \end{bmatrix} = \begin{bmatrix} 0.0698 \\ 0.0524 \\ 0.0349 \end{bmatrix}$$

$$[{}^B_F T] = \begin{bmatrix} 1.000 & 0.000 & 0.000 & 0.000 \\ 0.000 & 1.000 & 0.000 & 0.000 \\ 0.000 & 0.000 & 1.000 & 1.500 \\ 0 & 0 & 0 & 1 \end{bmatrix}, \begin{bmatrix} 0.750 & -0.216 & 0.625 & 0.000 \\ 0.433 & 0.875 & -0.216 & 0.000 \\ -0.500 & 0.433 & 0.750 & 1.500 \\ 0 & 0 & 0 & 1 \end{bmatrix}$$

3) Straight-Line Translation and Rotation

$$\begin{bmatrix} \dot{x} \\ \dot{y} \\ \dot{z} \end{bmatrix} = \begin{bmatrix} -0.005 \\ 0.030 \\ 0.060 \end{bmatrix} \quad \begin{bmatrix} \dot{\theta}_X \\ \dot{\theta}_Y \\ \dot{\theta}_Z \end{bmatrix} = \begin{bmatrix} 0.0698 \\ 0.0524 \\ 0.0349 \end{bmatrix}$$

$$[{}^B_F T] = \begin{bmatrix} 1.000 & 0.000 & 0.000 & 0.000 \\ 0.000 & 1.000 & 0.000 & 0.000 \\ 0.000 & 0.000 & 1.000 & 1.100 \\ 0 & 0 & 0 & 1 \end{bmatrix}, \begin{bmatrix} 0.750 & -0.216 & 0.625 & -0.050 \\ 0.433 & 0.875 & -0.216 & 0.300 \\ -0.500 & 0.433 & 0.750 & 1.700 \\ 0 & 0 & 0 & 1 \end{bmatrix}$$

Table I presents the number of iterations required at each time step for the simplified and exact forward position solutions, for the three simulations. The exact solution required a consistent number of iterations for all cases, either two or three. The simplified solution generally required a larger number of iterations. It performed better for the rotation case. The simplified solutions at the first computation step required more iterations to converge on the first solution from the relatively distant initial guess. The exact model does not display this behavior.

Table I: Number of Iterations for Forward Position Simulations

Simplified and Exact Models						
Step	1) Simp	1) Exact	2) Simp	2) Exact	3) Simp	3) Exact
1	11	2	16	2	11	2
2	9	2	1	3	9	3
3	9	2	3	3	7	3
4	9	2	2	3	7	3
5	9	2	2	3	6	3
6	9	2	2	3	5	3
7	9	2	2	3	4	3
8	9	2	2	3	4	3
9	9	2	2	3	4	3
10	8	2	2	3	4	3
11	8	2	2	3	3	3

The primary interest in the simplified model is less computations per iteration (compare Appendices B and C). An informal measure of computation time revealed little difference between the exact and simplified solution times. This is due to more iterations, plus the need to calculate $[{}^B T_s]$ using Eqs. 20, 21, 22, 11, 12, and 13. Therefore, based on Table I and the severe errors reported in Figs. 10c, 11c, and 12c, the simplified model is not an attractive alternative. The exact model has the additional advantage of providing the resolved rate solution with little additional calculation, based on the Newton-Raphson Jacobian matrix terms of Appendix C.

8 CONCLUSION

This paper presents the kinematic mathematical models for an in-parallel actuated robotic mechanism based on Stewart's platform. Position and velocity equations and solutions are given for a general platform. Examples and simulations are given for the Vehicle Emulator System (VES), a platform designed for NASA Langley by M.I.T. Equations in this paper are required for inverse position control and/or resolved rate (inverse velocity) control of the VES platform.

The inverse position solution is straight-forward and computationally inexpensive. Given the desired position and orientation of the moving platform with respect to the base, the lengths of the prismatic leg actuators are calculated.

The forward position solution is more complicated and theoretically has sixteen solutions. Two methods are pursued in this paper to solve this problem. Both use numerical solution techniques which produce one of the sixteen solutions; using the current position as an initial guess, the solution tracks the desired position. The first forward kinematics solution method is based on a simplified model where the six moving platform ball joints are grouped in three pairs. A fixed point iteration routine is used for solution of the basic equations. The second method is based on the exact VES platform model. A gradient-correction Newton-Raphson technique is used for solution.

The first forward kinematic model has inherent error due to the simplified platform model geometry. This method was pursued because of a perceived reduction in ^ρcomputation_Λ time. However, an informal measure of computation time revealed no significant difference between the two methods. A study of simplified model error shows that significant error results from the first solution technique. For these reasons, the second method using the Newton-Raphson technique is preferred, which yields the theoretically exact solution. In addition, the Newton-Raphson Jacobian matrix yields the platform inverse Jacobian matrix, with little modification. This represents a significant computation savings

for resolved rate control.

The velocity kinematics section presents the resolved rate solution. Given the desired Cartesian velocity of the end-effector, the required leg actuator rates are calculated. As mentioned above, the Newton-Raphson Jacobian matrix resulting from the second forward position kinematics solution is a modified inverse Jacobian matrix. The relationship between the modified and actual Jacobian matrices is given. For the resolved rate solution, no matrix inversion is required because the inverse matrix is calculated directly from platform geometry in the forward position kinematics Newton-Raphson solution. The parallel platform is free of singularities in the resolved rate control method. In contrast, most serial industrial manipulators have several singularities which degrade overall performance.

Static examples are given to demonstrate calculations of the various equations of this paper. Translation and rotation motions are studied in ten second simulations to demonstrate the leg inputs, the forward position solution convergence, and the simplified forward position model error for the platform under inverse position or resolved rate control.

9 REFERENCES

Craig, J.J., *Introduction to Robotics: Mechanics and Control*, Addison Wesley Publishing Co., Reading, MA, 1988.

Cwiakala, M., "Workspace of a Closed-Loop Manipulator", ASME Paper 86-DET-95, 1986.

Dahlquist, G., and Bjorck, A., *Numerical Methods*, Prentice-Hall, Inc., Englewood Cliffs, NJ, 1974.

Dieudonne, J.E., Parrish, R.V., and Bardusch, R.E., "An Actuator Extension Transformation for a Motion Simulator and an Inverse Transformation Applying Newton-Raphson's Method", NASA Technical Note TN D-7067, Langley Research Center, November, 1972.

Fichter, E.F., "A Stewart Platform-Based Manipulator: General Theory and Practical Construction", *International Journal of Robotics Research*, Vol. 5, No. 2, 1986, pp. 157-182.

Hunt, K.H., "Structural Kinematics of In-Parallel Actuated Robot Arms", *Journal of Mechanisms, Transmissions, and Automation in Design*, Vol. 105, No. 4, December 1983, pp. 705-712.

Kane, T.R., Likins, P.W., and Levinson, D.A., *Spacecraft Dynamics*, McGraw-Hill Book Co., New York, 1983.

Mabie, H.H., and Reinholtz, C.F., *Mechanisms and Dynamics of Machinery*, John Wiley & Sons, New York, 1987.

Nanua, P., Waldron, K. J., and Murthy, V., "Direct Kinematic Solution of a Stewart Platform", *IEEE Transactions on Robotics and Automation*, Vol. 6, No. 4, August 1990, pp. 438-443.

Nguyen, C.C., Zhou, Z., Antrazi, S.S, and Campbell, C.E., "Efficient Computation of Forward Kinematics and Jacobian Matrix of a Stewart Platform-Based Manipulator", *Proceedings of the IEEE Southeastcon '91*, April 1991.

Powell, I., "The Kinematic Analysis and Simulation of the Parallel Topology Manipulator", *The Marconi Review*, Vol. 45, No. 226, 3rd Quarter 1982, pp. 121-138.

Press, W.H., Flannery, B.P., Teukolsky, S.A., and Vetterling, W.T., *Numerical Recipes: The Art of Scientific Computing*, Cambridge University Press, Cambridge, 1986.

Salmon, G., *Lessons Introductoru to the Modern Higher Algebra (5th Ed.)*, Chelsea, New York, 1964.

Stewart, D., "A Platform with Six Degrees of Freedom", *Proceedings of the Institute of Mechanical Engineers (London)*, Vol. 180, Part 1, No. 15, 1965-66, pp. 371-386.

Sugimoto, K., "Kinematic and Dynamic Analysis of Parallel Manipulators by means of Motor Algebra", *Journal of Mechanisms, Transmissions, and Automation in Design*, Vol. 109, 1987, pp. 3-7.

Watson, L.T., "Globally Convergent Homotopy Algorithms for Nonlinear Systems of Equations", *TR 90-26*, Department of Computer Science, Virginia Polytechnic Institute and State University, Blacksburg, VA, 1990.

Williams, R. L., "Planar Robotic Mechanisms: Analysis and Configuration Comparison", Doctoral Dissertation, Department of Mechanical Engineering, Virginia Polytechnic Institute and State University, Blacksburg, VA, 1988.

Yang, D.C.H, and Lee, T.W., "Feasibility Study of a Platform Type of Robotic Manipulator from a Kinematic Viewpoint", *Journal of Mechanisms, Transmissions, and Automation in Design*, Vol. 106, No. 2, June 1984, pp. 191-198.

APPENDIX A: FIXED PLATFORM PARAMETERS

This appendix presents nominal geometric parameters for the VES platform. The following are the ball joint locations of the fixed base, expressed in $\{B\}$. The units for all terms in this appendix are *mm*.

$$\begin{aligned}
 {}^B\mathbf{V}_{B1} &= \begin{Bmatrix} 1338.1 \\ 76.2 \\ 0.0 \\ 1.0 \end{Bmatrix} &
 {}^B\mathbf{V}_{B2} &= \begin{Bmatrix} -603.0 \\ 1197.1 \\ 0.0 \\ 1.0 \end{Bmatrix} &
 {}^B\mathbf{V}_{B3} &= \begin{Bmatrix} -735.1 \\ 1120.9 \\ 0.0 \\ 1.0 \end{Bmatrix} \\
 {}^B\mathbf{V}_{B4} &= \begin{Bmatrix} -735.1 \\ -1120.9 \\ 0.0 \\ 1.0 \end{Bmatrix} &
 {}^B\mathbf{V}_{B5} &= \begin{Bmatrix} -603.0 \\ -1197.1 \\ 0.0 \\ 1.0 \end{Bmatrix} &
 {}^B\mathbf{V}_{B6} &= \begin{Bmatrix} 1338.1 \\ -76.2 \\ 0.0 \\ 1.0 \end{Bmatrix}
 \end{aligned}$$

The vectors below are the ball joint locations of the moving platform, expressed in $\{P\}$.

$$\begin{aligned}
 {}^P\mathbf{V}_{P1} &= \begin{Bmatrix} 213.6 \\ 217.4 \\ 0.0 \\ 1.0 \end{Bmatrix} &
 {}^P\mathbf{V}_{P2} &= \begin{Bmatrix} 81.5 \\ 293.6 \\ 0.0 \\ 1.0 \end{Bmatrix} &
 {}^P\mathbf{V}_{P3} &= \begin{Bmatrix} -295.1 \\ 76.2 \\ 0.0 \\ 1.0 \end{Bmatrix} \\
 {}^P\mathbf{V}_{P4} &= \begin{Bmatrix} -295.1 \\ -76.2 \\ 0.0 \\ 1.0 \end{Bmatrix} &
 {}^P\mathbf{V}_{P5} &= \begin{Bmatrix} 81.5 \\ -293.6 \\ 0.0 \\ 1.0 \end{Bmatrix} &
 {}^P\mathbf{V}_{P6} &= \begin{Bmatrix} 213.6 \\ -217.4 \\ 0.0 \\ 1.0 \end{Bmatrix}
 \end{aligned}$$

Vectors below are the ball joint locations of the moving platform for the simplified forward position kinematics model, expressed in $\{P\}$.

$${}^P\mathbf{V}_{Q1} = \begin{Bmatrix} 152.4 \\ 263.9 \\ 0.0 \\ 1.0 \end{Bmatrix} \quad
 {}^P\mathbf{V}_{Q2} = \begin{Bmatrix} -304.8 \\ 0.0 \\ 0.0 \\ 1.0 \end{Bmatrix} \quad
 {}^P\mathbf{V}_{Q3} = \begin{Bmatrix} 152.4 \\ -263.9 \\ 0.0 \\ 1.0 \end{Bmatrix}$$

The lengths a_i and $b_i, i = 1, 2, 3$ are fixed lengths separating ball joints in the moving platform and the fixed base, respectively. These terms are defined in Eqs. 5a and 5b.

$$\begin{aligned}
 a_1 &= a_2 = a_3 = 528.0 \\
 b_1 &= b_2 = b_3 = 2242.0
 \end{aligned}$$

The ball joints of the moving platform and the fixed base lie on circles of radii r_P and r_B , respectively. These radii are measured from the origins of $\{P\}$ and $\{B\}$. They are required in Eqs. 34.

$$\begin{aligned}
 r_P &= 305.0 \\
 r_B &= 1340.0
 \end{aligned}$$

APPENDIX B: FORWARD POSITION SOLUTION FOR SIMPLIFIED MODEL

There is no general method suitable for solving every non-linear system of equations. In this appendix, a conceptually simple one-point iteration numerical method (Dahlquist and Bjorck (1974), Section 6.9.1) is presented to simultaneously solve Eqs. 14, 15, and 16, derived from the simplified forward position kinematics model.

Let the following represent a non-linear system of n equations in n unknowns.

$$F_i(\mathbf{X}) = 0; \quad i = 1, 2, \dots, n \quad (B.1)$$

where:

$$\mathbf{X} = \{x_1, x_2, \dots, x_n\}^T$$

The one-point iteration method requires that each of the n equations be symbolically solved for a different unknown to yield:

$$x_j = f_j(\hat{\mathbf{X}}); \quad j = 1, 2, \dots, n \quad (B.2)$$

where:

$$\hat{\mathbf{X}} = \{x_i\}^T; i \neq j$$

Starting from an initial guess for \mathbf{X} , Eqs. B.2 are calculated iteratively, updating each x_j for subsequent use. The convergence criteria for this method is given in Dahlquist and Bjorck (1974, Section 6.9.1). The convergence of this method is linear.

Equations 14, 15, and 16 are three transcendental equations in the three unknowns $\theta_1, \theta_2, \theta_3$. In order to facilitate writing them in the form of Eq. B.2, they are viewed as three equations in the six unknowns $c_i, s_i; i = 1, 2, 3$. The unknowns $c_i; i = 1, 2, 3$ are solved from Eqs. 14, 15, and 16, respectively.

$$c_1 = \frac{-D_2 c_2 - D_4 s_1 s_2 - D_5}{D_1 + D_3 c_2} \quad (B.3)$$

$$c_2 = \frac{-E_2 c_3 - E_4 s_2 s_3 - E_5}{E_1 + E_3 c_3} \quad (B.4)$$

$$c_3 = \frac{-F_2 c_1 - F_4 s_3 s_1 - F_5}{F_1 + F_3 c_1} \quad (B.5)$$

The remaining unknowns $s_i; i = 1, 2, 3$ are related to the c_i terms through $c_i^2 + s_i^2 = 1$. This yields three constraint equations, written to isolate the s_i unknowns.

$$s_1 = \sqrt{1 - c_1^2} \quad (B.6)$$

$$s_2 = \sqrt{1 - c_2^2} \quad (B.7)$$

$$s_3 = \sqrt{1 - c_3^2} \quad (B.8)$$

With a suitable initial guess as the starting point, Eqs. B.3 through B.8 are used for iteration, continuously updating $c_i, s_i; i = 1, 2, 3$. In using this method for practical platform control, the previous solution constitutes an excellent initial guess. For the first time step, a designated reset position is the initial guess. At the reset position introduced in Section 5, the angles $\theta_i, i = 1, 2, 3$ are $\{73.8^\circ, 73.8^\circ, 73.8^\circ\}^T$. These values are approximate due to the simplified model error, discussed in Sections 3.2.1 and 6. The iteration continues until the change between each successive c_i, s_i is sufficiently small.

$$|\text{MAX}(c_i - c_{i_{PREV}})| < \epsilon \quad (B.9a)$$

$$|\text{MAX}(s_i - s_{i_{PREV}})| < \epsilon \quad (B.9b)$$

where $i = 1, 2, 3$ and ϵ is a user-defined tolerance. In practical implementation of this algorithm, convergence was achieved even for distant initial guesses.

The unknown angles θ_i are obtained from the solved values of c_i .

$$\theta_i = \cos^{-1}(c_i) \quad i = 1, 2, 3 \quad (B.10)$$

The inverse cosine function is double-valued, yielding $\pm\theta_i$. Only the positive angles are admissible due to VES platform workspace limits, as evident in Fig. 6. All three angles are confined to the first quadrant, $0 \leq \theta_i \leq 90^\circ$. Due to mechanical limits, the angles are restricted significantly further than this, $65.4^\circ \leq \theta_i \leq 77.5^\circ$.

Given the three intermediate angles, the simplified model approximation to the forward position kinematic solution, ${}^B_P T_s$, is calculated using Eqs. 20, 21, 22, 11, 12, and 13.

APPENDIX C: FORWARD POSITION SOLUTION FOR EXACT MODEL

This appendix presents a solution method for the exact model forward position kinematics problem. As observed in Appendix B, there is no general method for solving non-linear systems of equations. In this appendix the well known Newton-Raphson method is used to solve Eqs. 34. This is a first order gradient correction method. The following presentation is adapted from Press, et. al. (1986, Section 9.6).

Let the following represent a non-linear system of n equations in n unknowns.

$$F_i(\mathbf{X}) = 0; \quad i = 1, 2, \dots, n \quad (C.1)$$

where:

$$\mathbf{X} = \{x_1, x_2, \dots, x_n\}^T$$

The above equations are expanded in a Taylor series about the neighborhood of \mathbf{X} . Neglecting the quadratic and higher terms, a linear system of equations results. The details are in Press, et. al. (1986, Section 9.6).

$$[J]\{\delta\mathbf{X}\} = -\{F_i(\mathbf{X})\} \quad (C.2)$$

The unknown vector $\{\delta\mathbf{X}\}$ is the first order gradient correction for the current \mathbf{X} vector. The right hand side of Eq. C.2 is the negative of the non-linear functions (Eq. C.1) evaluated at the current \mathbf{X} . The matrix $[J]$ is a Jacobian matrix, a multi-dimensional form of the derivative.

$$[J] = \left[\frac{\partial F_i}{\partial x_j} \right] \quad (C.3)$$

The process requires an initial guess for \mathbf{X} . For each iteration, the update equation is Eq. C.4. Iteration continues until the largest component of the correction vector is less than a user-specified tolerance, as shown in Eq. C.5. The convergence criteria for the Newton-Raphson method is given in Dahlquist and Bjorck (1974, Section 6.9.2). There is

a quadratic convergence, which yields convergence in less steps than the linear convergence of Appendix B.

$$\mathbf{X}_{n+1} = \mathbf{X}_n + \delta\mathbf{X} \quad (C.4)$$

$$\text{MAX}(|\delta\mathbf{X}_i|) < \epsilon \quad (C.5)$$

Where ϵ is a user-defined tolerance (separate position and orientation criterion may be defined), with a different interpretation than that of Appendix B. The tolerance of Appendix B is a limit on the change in successive sines and cosines of the angle $\theta_i, i = 1, 2, 3$ in Fig 6. The tolerance in the present method represents the precision for the Cartesian values comprising ${}^B_P T$, $\mathbf{X} = \{x, y, z, \theta_x, \theta_y, \theta_z\}^T$.

The exact model forward position kinematics problem requires the solution of Eqs. 34. Unlike the simplified model solution method presented in Appendix B, the exact solution variables describe elements of ${}^B_P T$. As in Appendix B, the first initial guess should be a reset position where the forward solution is known. The current VES platform ${}^B_P T$ is a good initial guess for the next control cycle, during subsequent motion.

The initial guess for a control cycle is of the following form.

$$\{\mathbf{X}_0\} = \{x_0, y_0, z_0, \theta_{x0}, \theta_{y0}, \theta_{z0}\}^T$$

At reset, $\{\mathbf{X}_0\}$ is $\{0, 0, 1.531, 0, 0, 0\}^T$ (see Section 5, Example 1b). With practical implementation of the Newton-Raphson method, convergence was achieved even for relatively distant initial guesses.

For the VES platform, the non-linear functions of Eq. C.1 have identical form, Eq. 34. The only parameters which change are the fixed base and moving platform ball joint locations. Therefore, each row of the Newton-Raphson Jacobian matrix has the same form,

given in Eq. C.6.

$$\begin{aligned}
J_{NR}(i, 1) &= 2[x + P_{ix}r_{11} + P_{iy}r_{12} - B_{ix}] \\
J_{NR}(i, 2) &= 2[y + P_{ix}r_{21} + P_{iy}r_{22} - B_{iy}] \\
J_{NR}(i, 3) &= 2[z + P_{ix}r_{31} + P_{iy}r_{32}] \\
J_{NR}(i, 4) &= 2[P_{iy}r_{13}(x - B_{ix}) + P_{iy}r_{23}(y - B_{iy}) + P_{iy}r_{33}z] \\
J_{NR}(i, 5) &= 2[(-P_{ix}s_y c_z + P_{iy}r_{32}c_z)(x - B_{ix}) + (-P_{ix}s_y s_z + P_{iy}r_{32}s_z)(y - B_{iy}) + (-P_{ix}c_y - P_{iy}s_x s_y)z] \\
J_{NR}(i, 6) &= 2[-(P_{ix}r_{21} + P_{iy}r_{22})(x - B_{ix}) + (P_{ix}r_{11} + P_{iy}r_{12})(y - B_{iy})]
\end{aligned} \tag{C.6}$$

The subscript NR is used to distinguish the Newton-Raphson Jacobian matrix from the VES platform Jacobian matrix. As derived in Section 4, J_{NR} is related to the inverse of the VES platform Jacobian matrix.

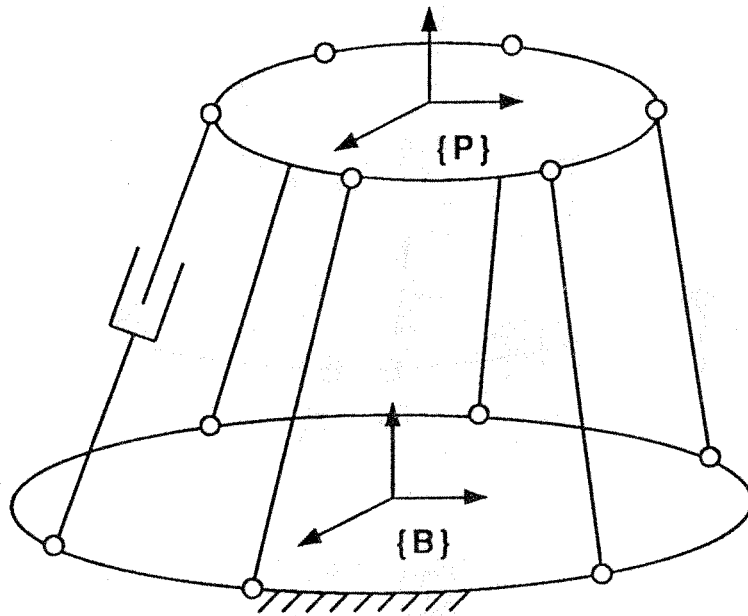


Figure 1
General Platform
Kinematic Diagram

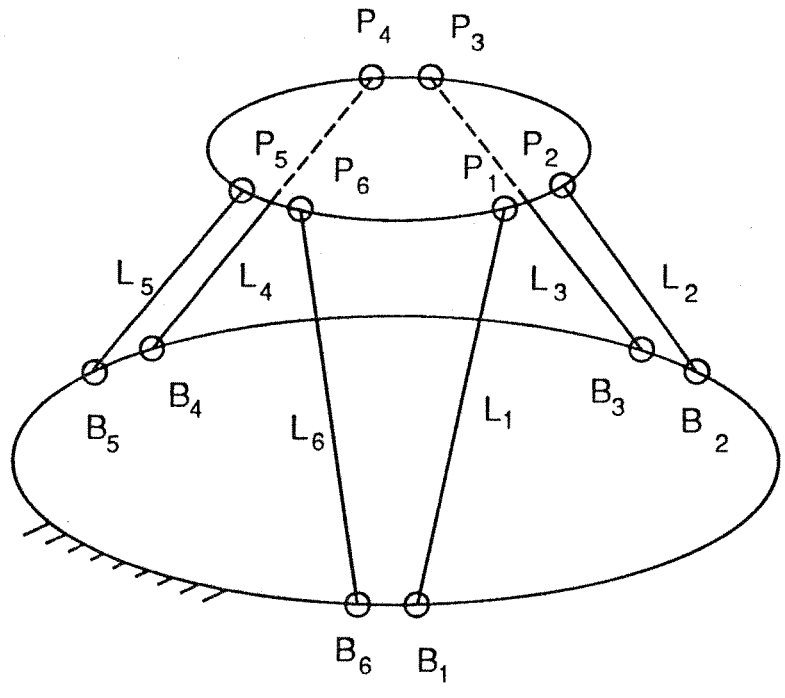


Figure 2
VES Platform
Kinematic Diagram

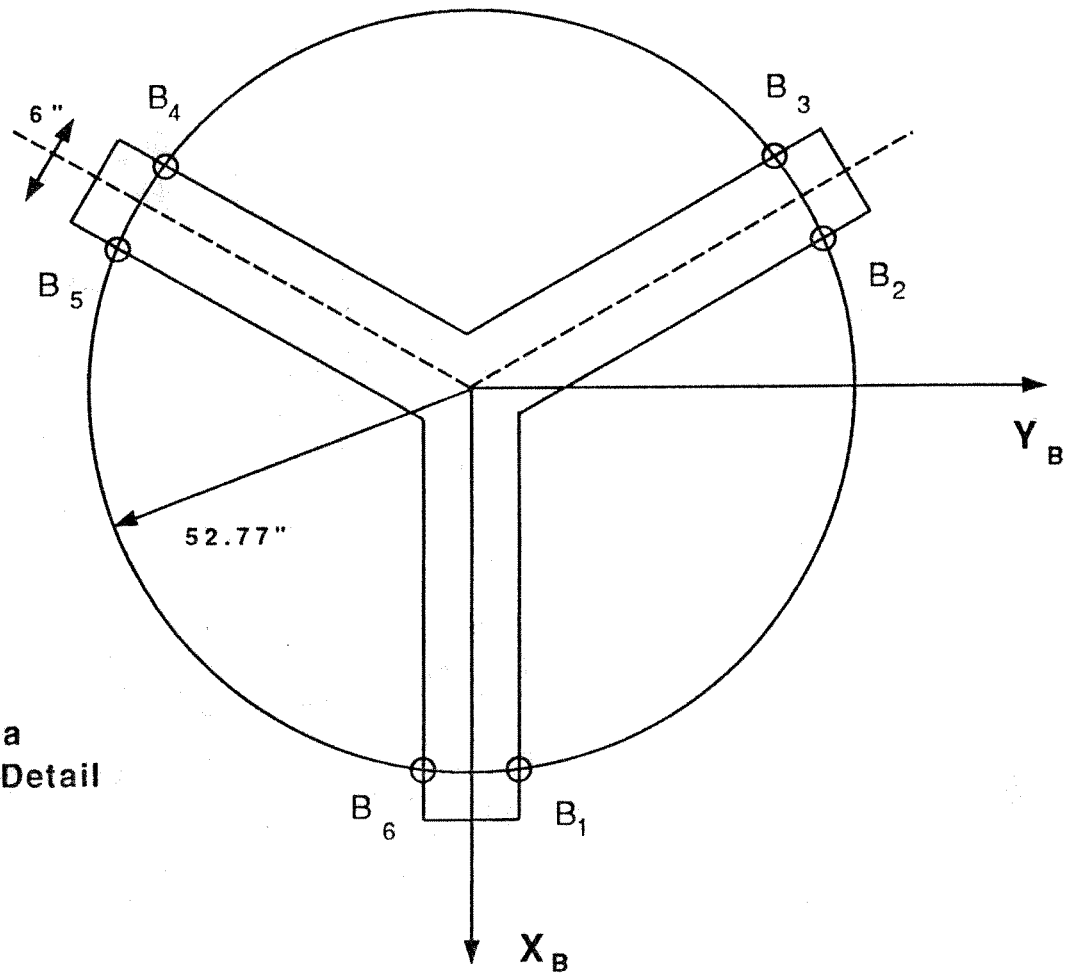


Figure 3a
Fixed Base Detail

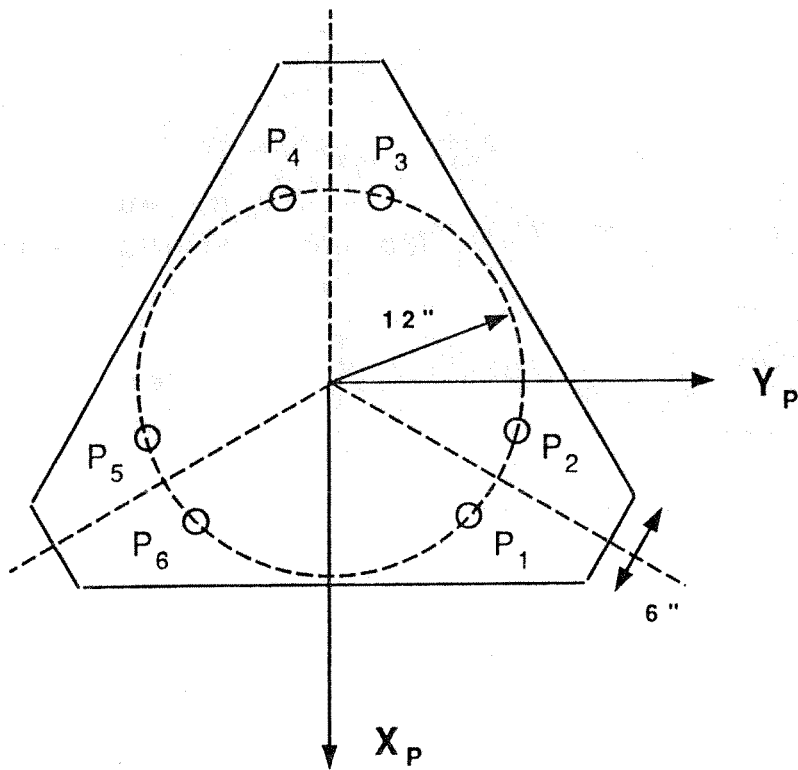


Figure 3b
Moving Platform Detail

Figure 3
VES Platform
Ball Joint Geometry

Figure 4a
Kinematic Diagram

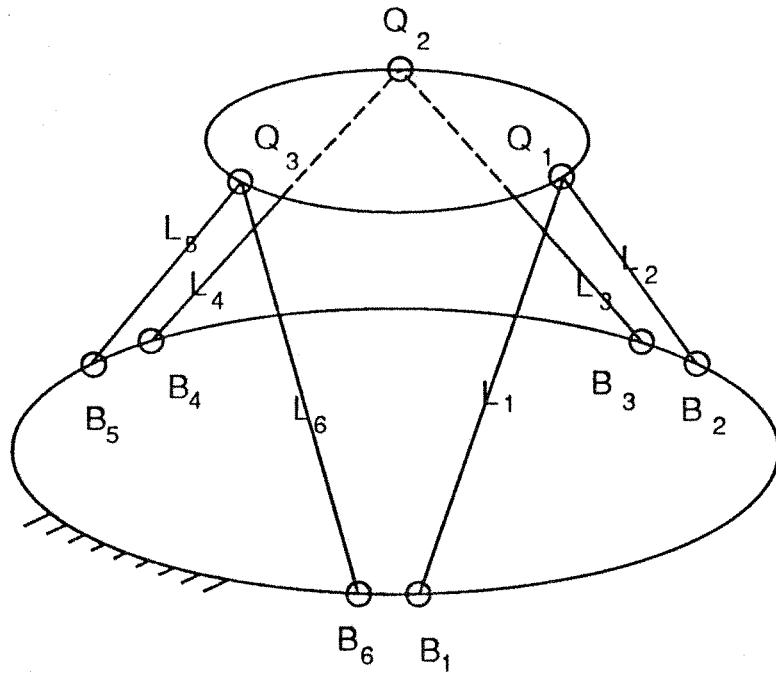


Figure 4b
Moving Platform Detail

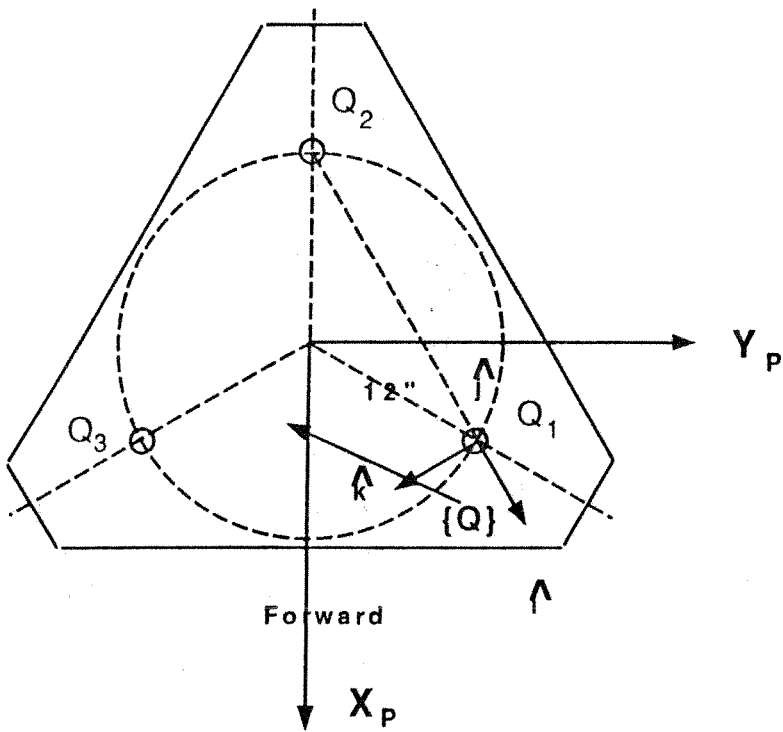


Figure 4
Simplified VES Platform Model

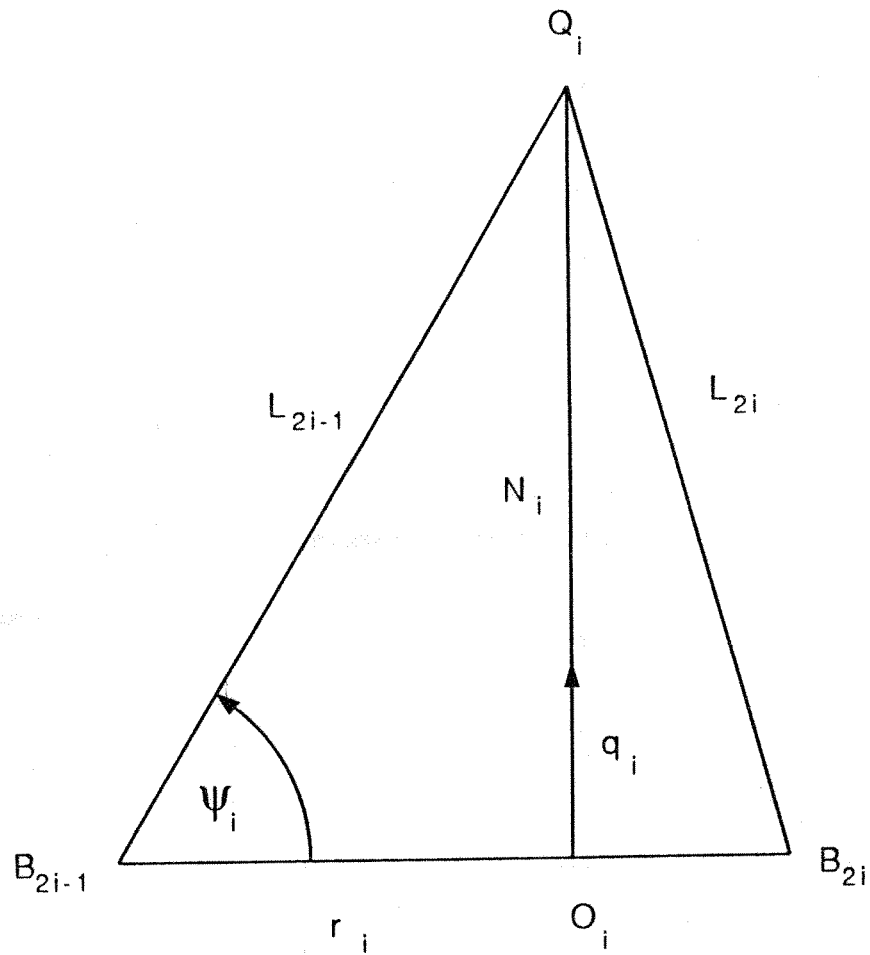


Figure 5
General B-Q-B-B Chain
in VES Platform Simplified Model

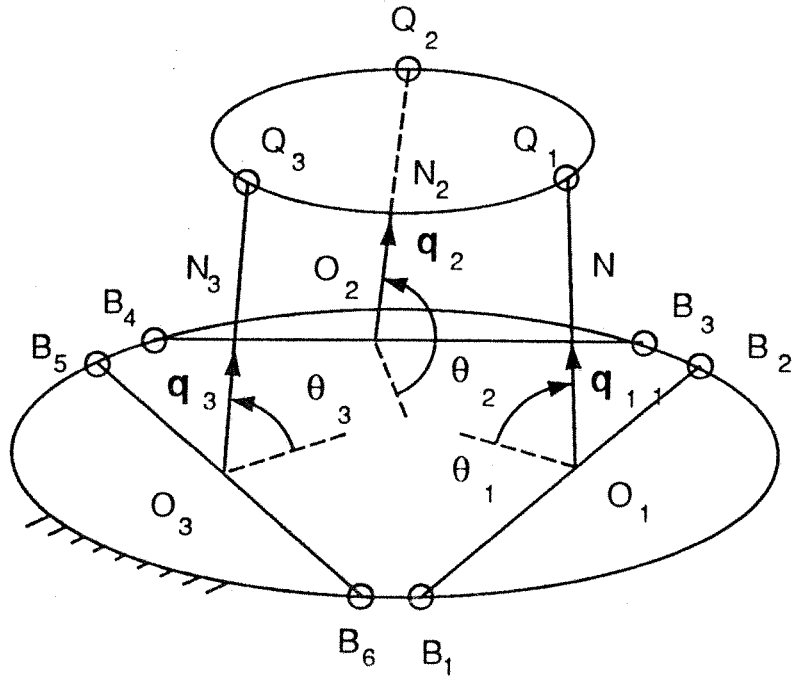


Figure 6
 VES Platform
 Reduced Simplified
 Kinematic Diagram

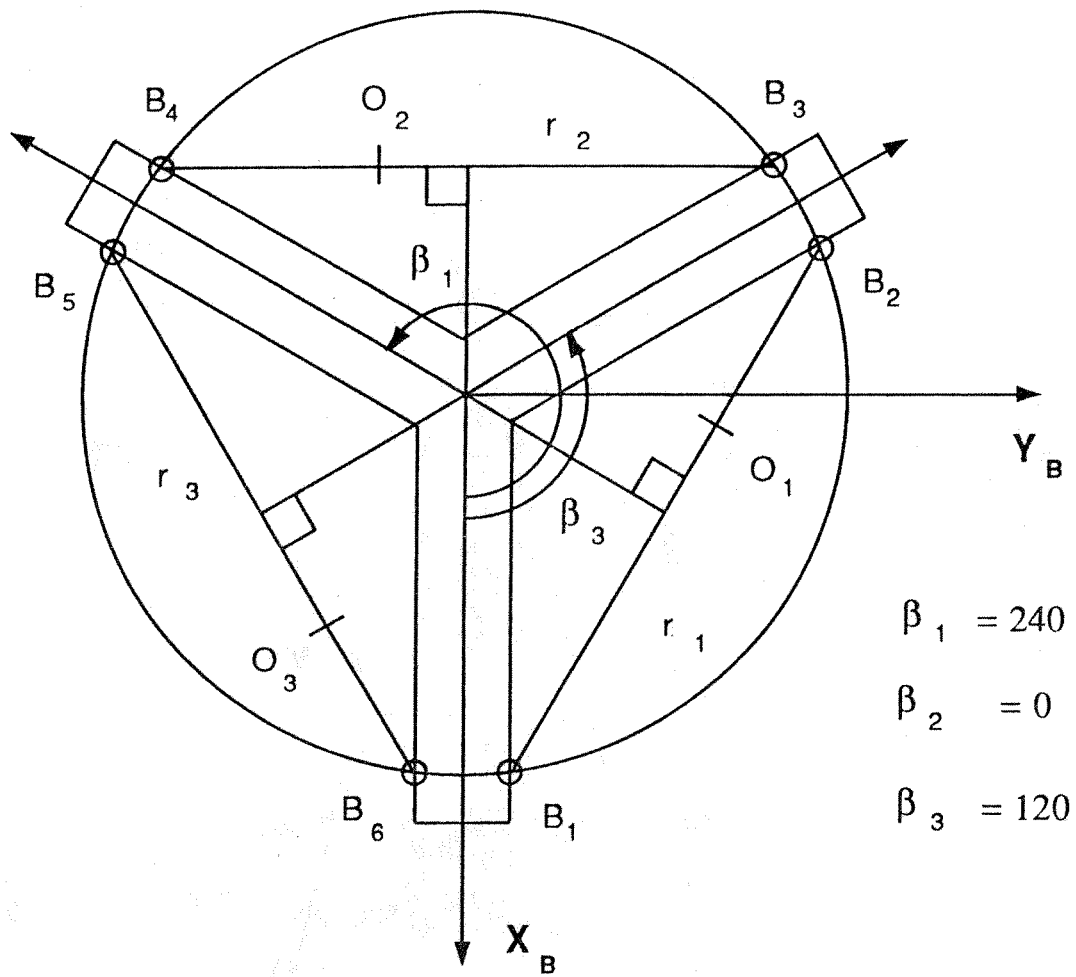


Figure 7
 Definition of β_i
 On the VES Platform Base

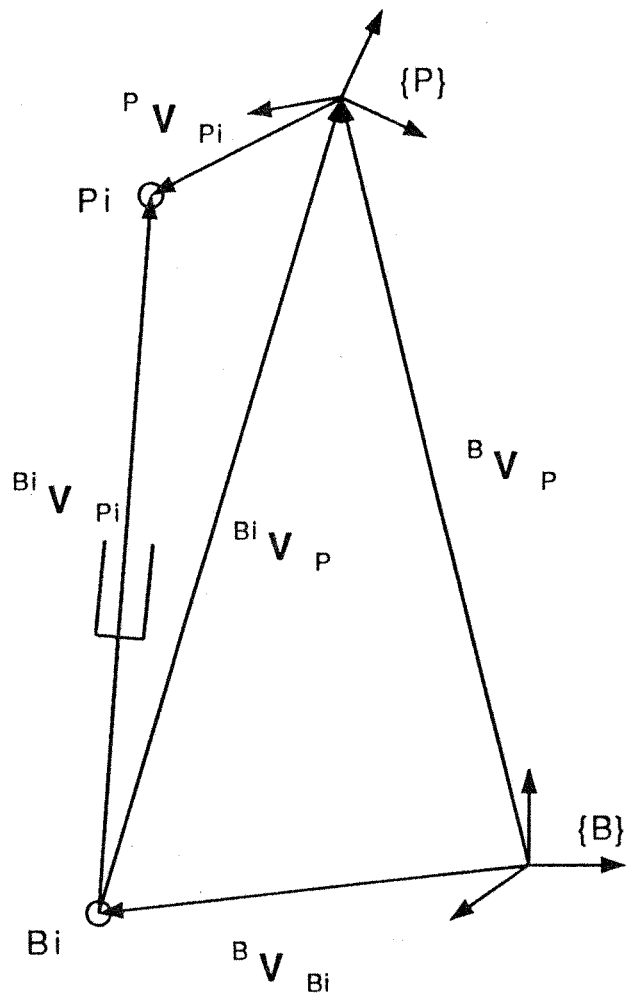


Figure 8
Kinematic Diagram for the i th Actuator
of the VES Platform

Figure 9
VES Platform Vertical Translation,
Equal Leg Lengths

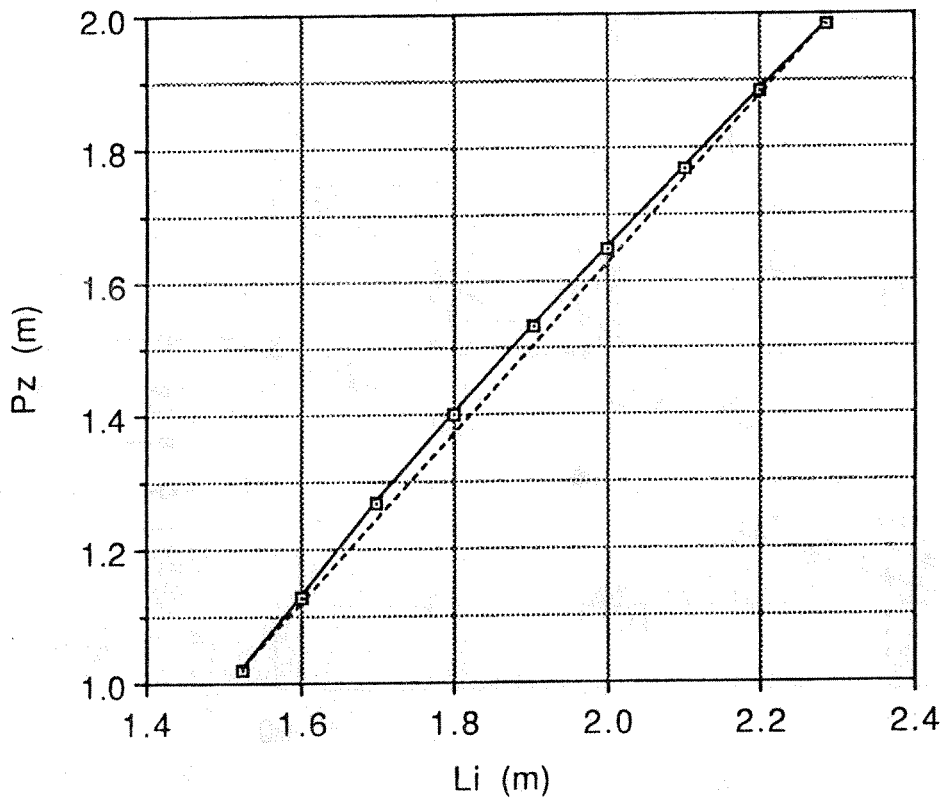


Figure 10a
Inverse Position Solution
VES Translation Simulation

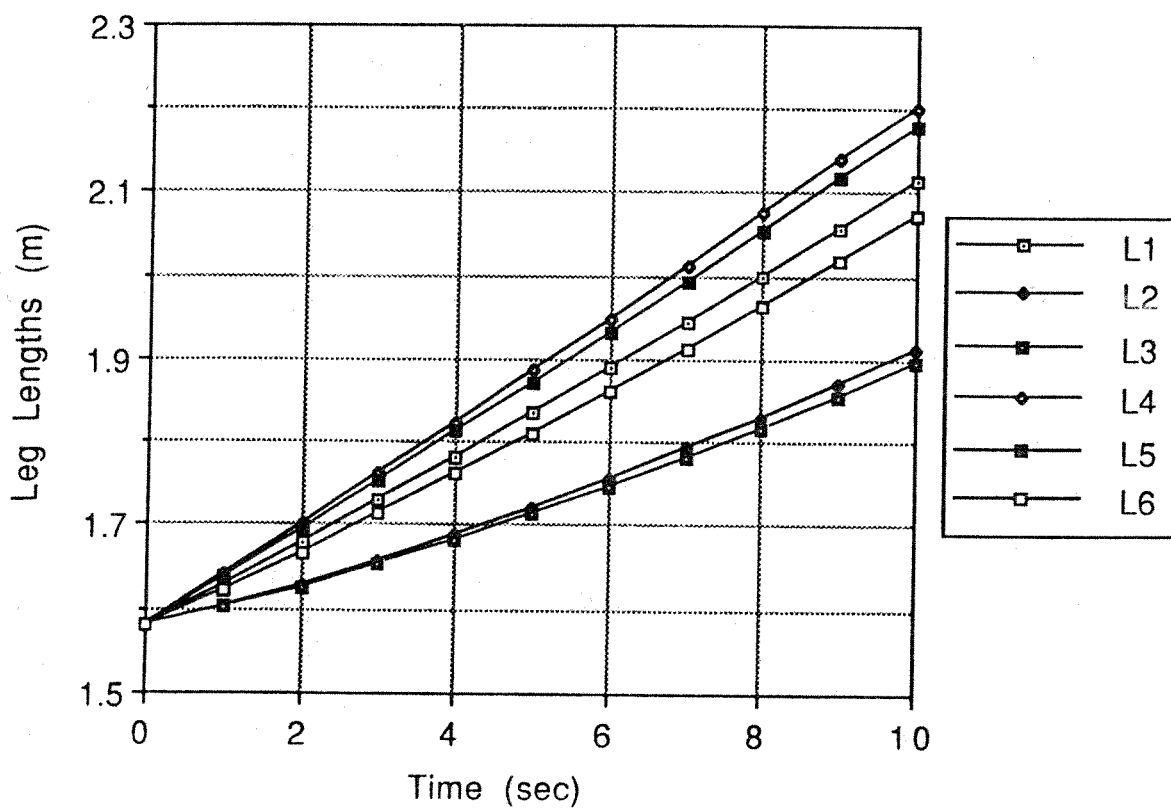


Figure 10b
Resolved Rate Solution
VES Translation Simulation

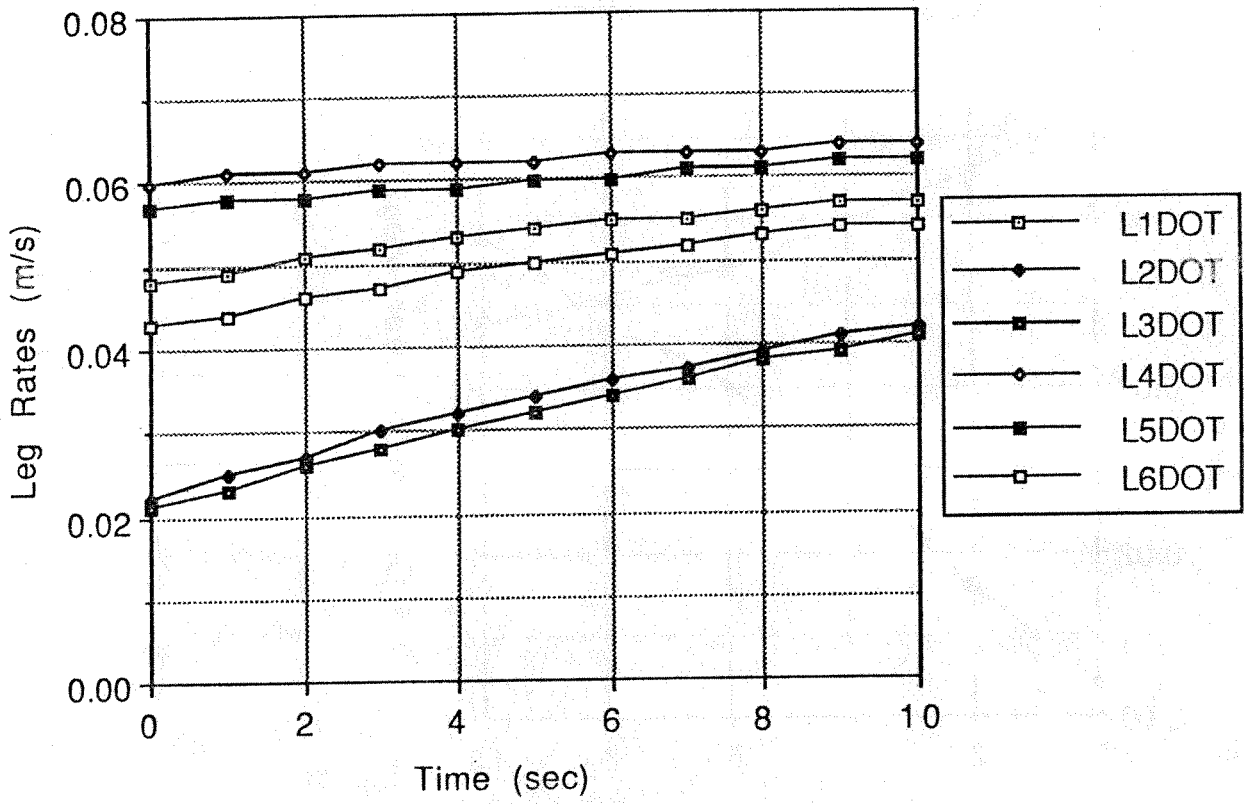


Figure 10c
Simplified Forward Model Error
VES Translation Simulation

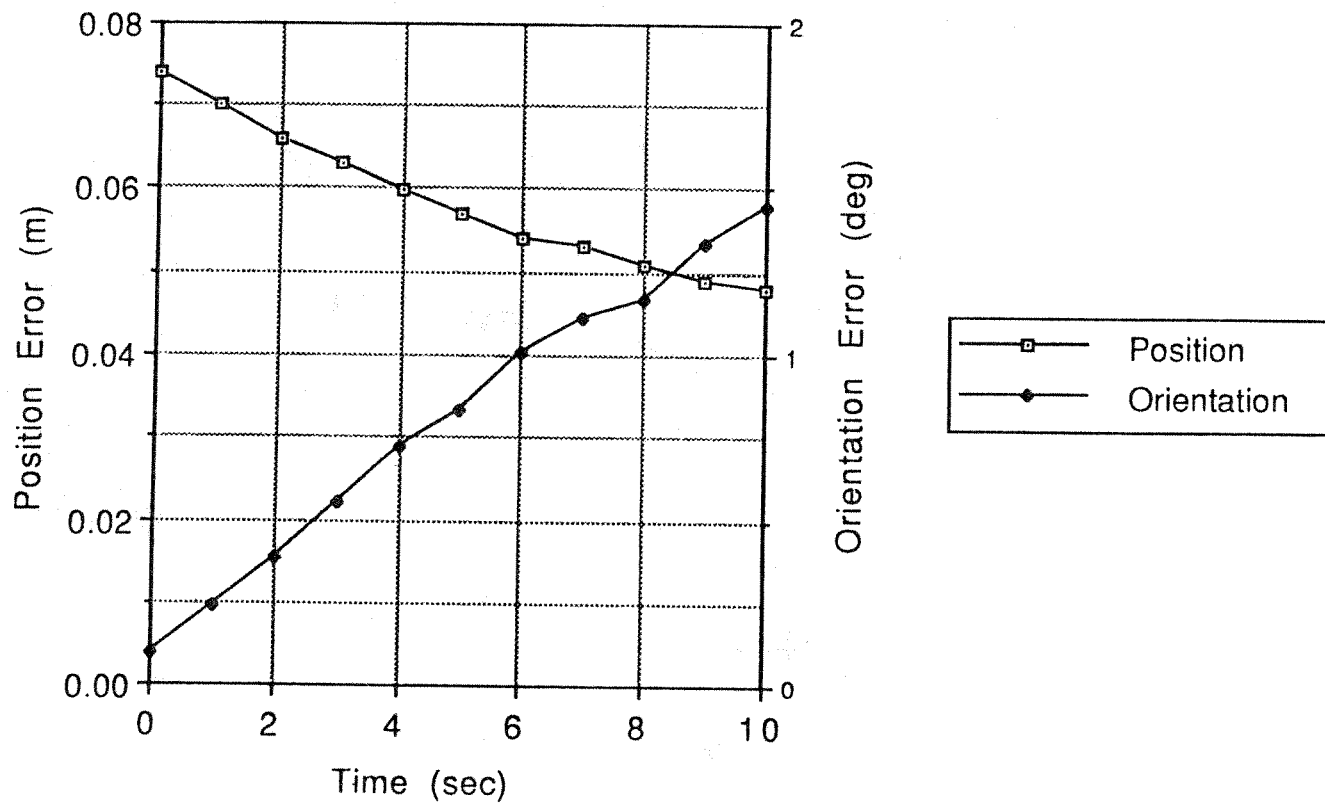


Figure 11a
Inverse Position Solution
VES Rotation Simulation

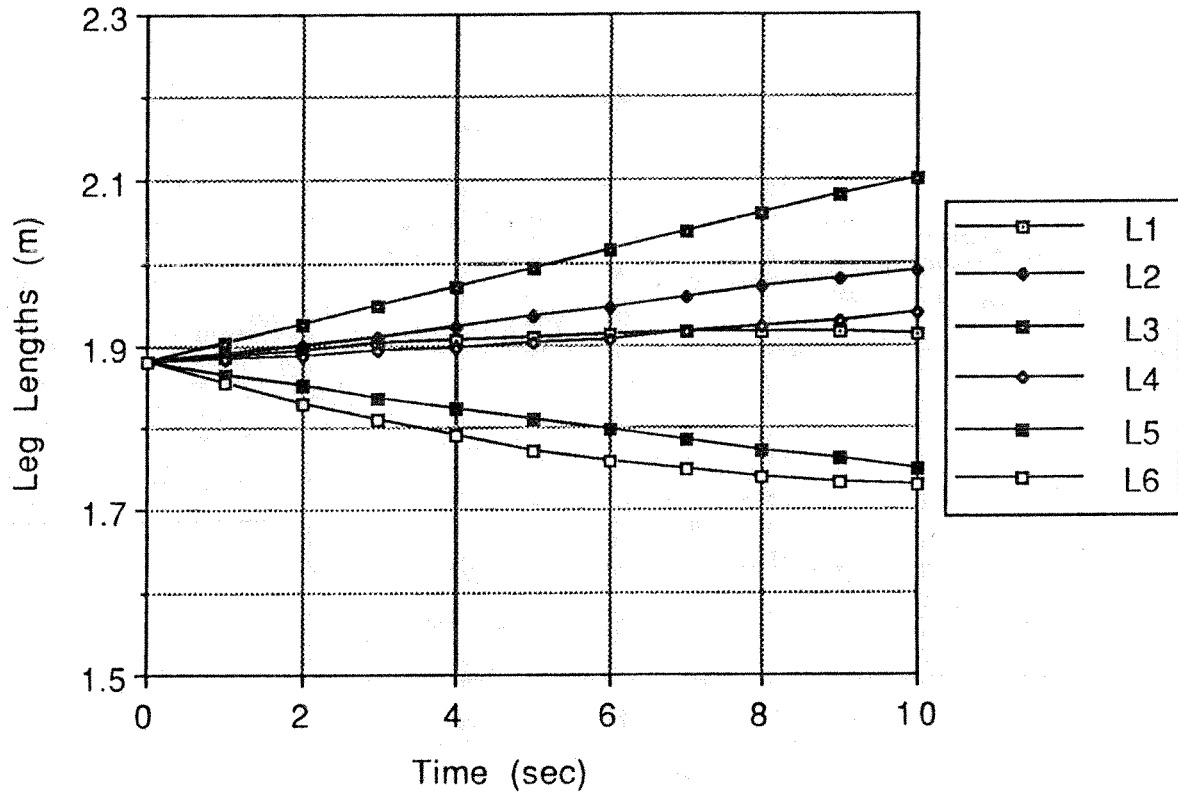


Figure 11b
Resolved Rate Solution
VES Rotation Simulation

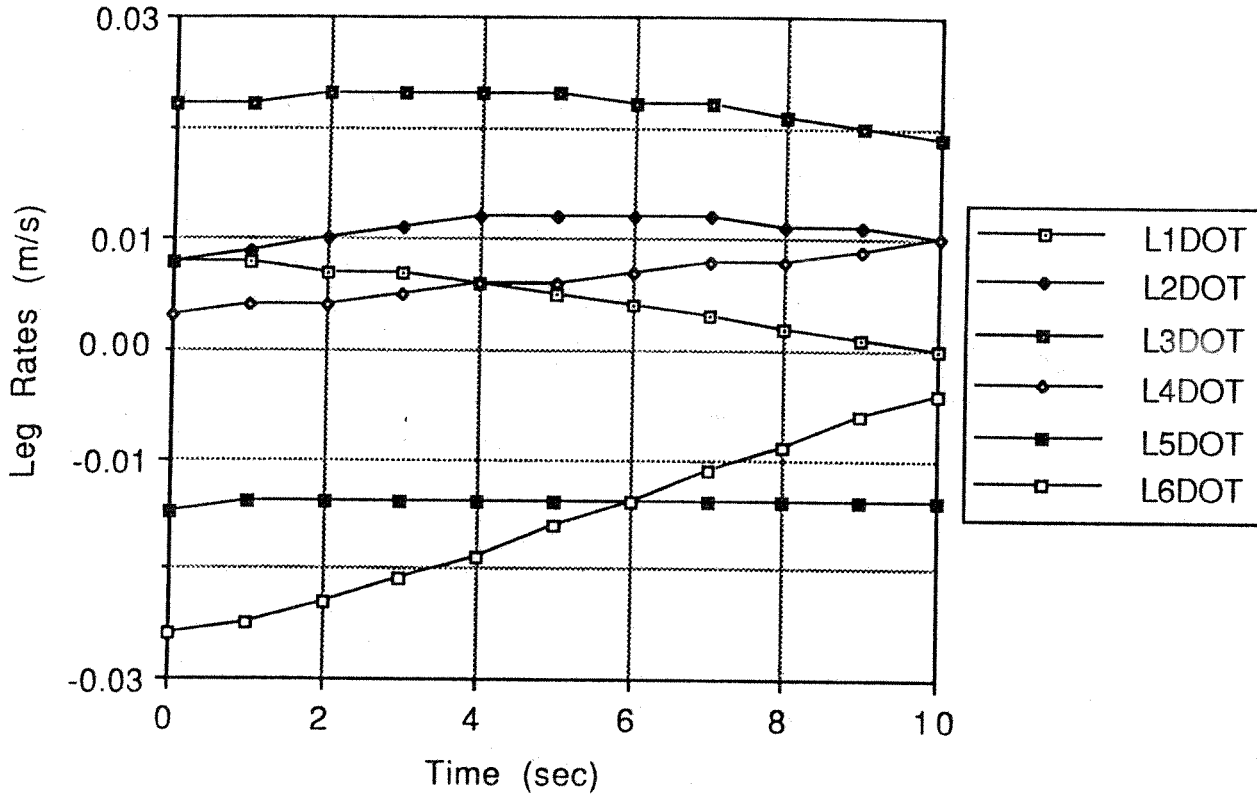


Figure 11c
Simplified Forward Model Error
VES Rotation Simulation

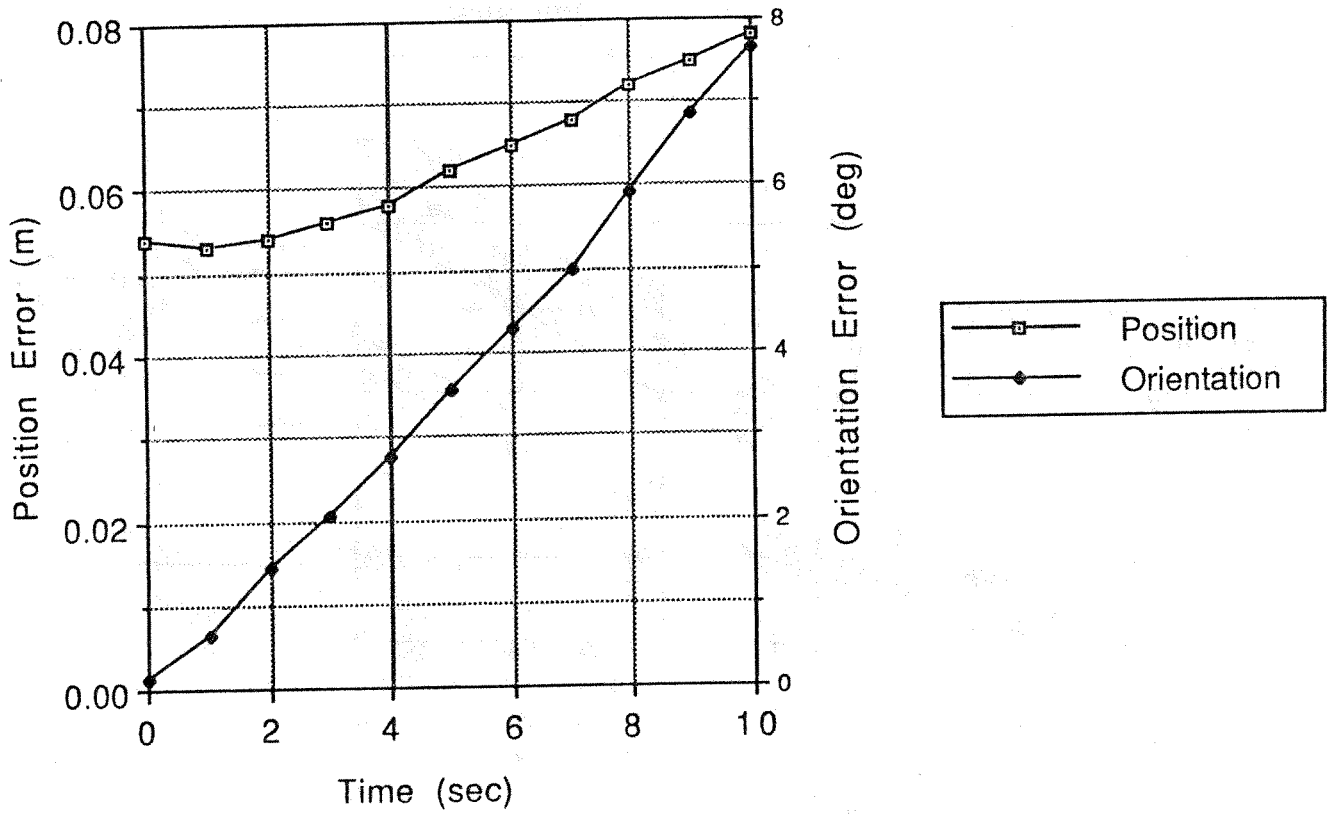


Figure 12a
Inverse Position Solution
VES Translation/Rotation Simulation

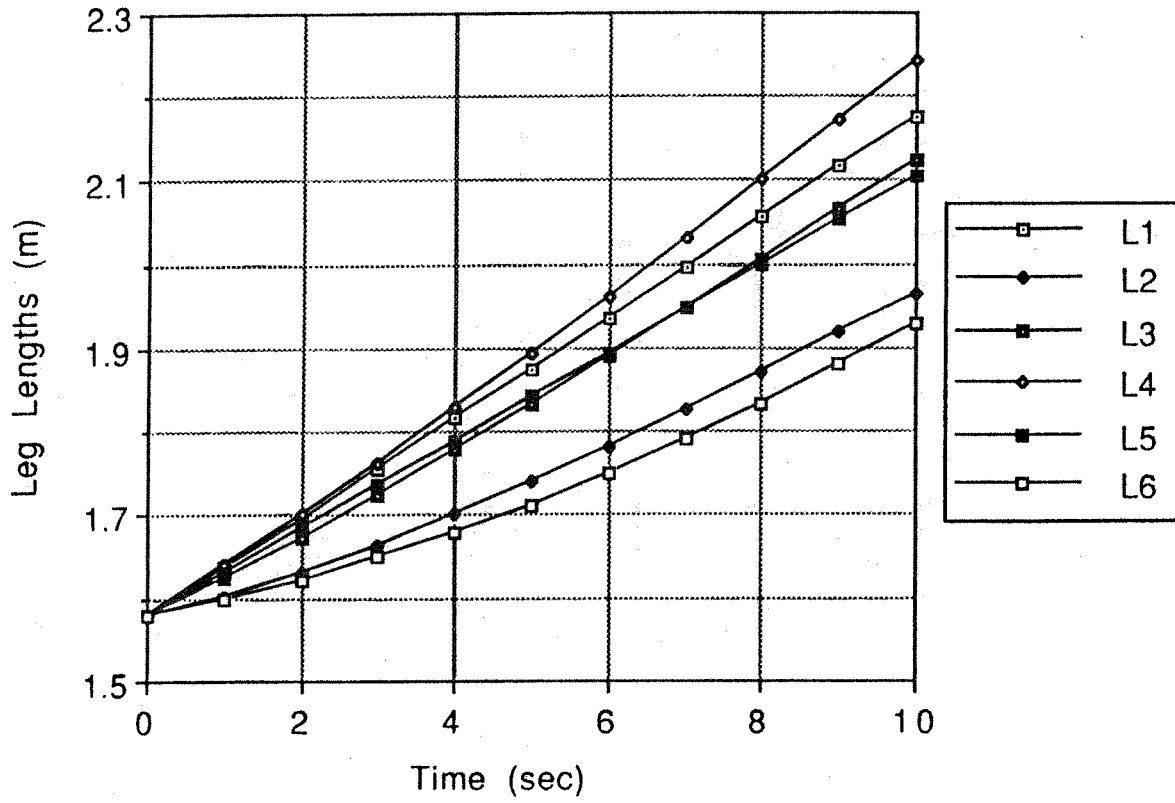


Figure 12b
Resolved Rate Solution
VES Translation/Rotation Simulation

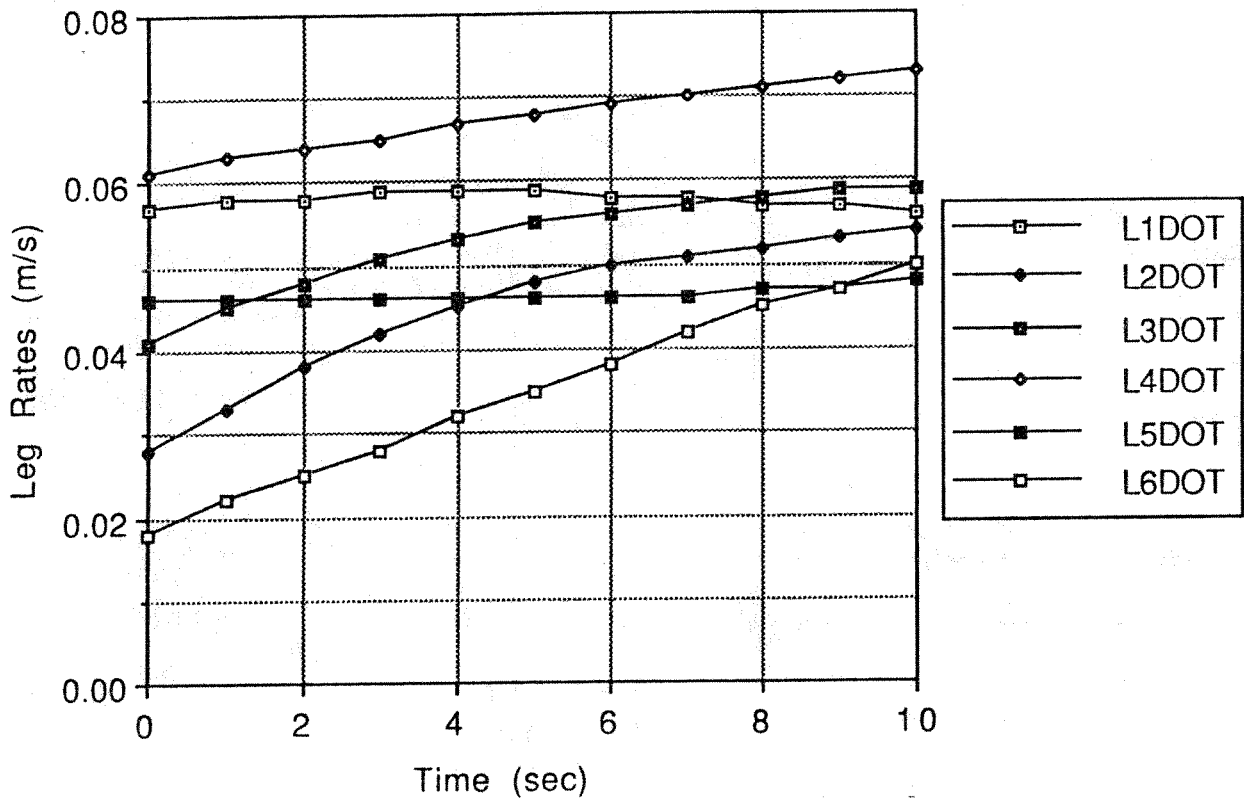
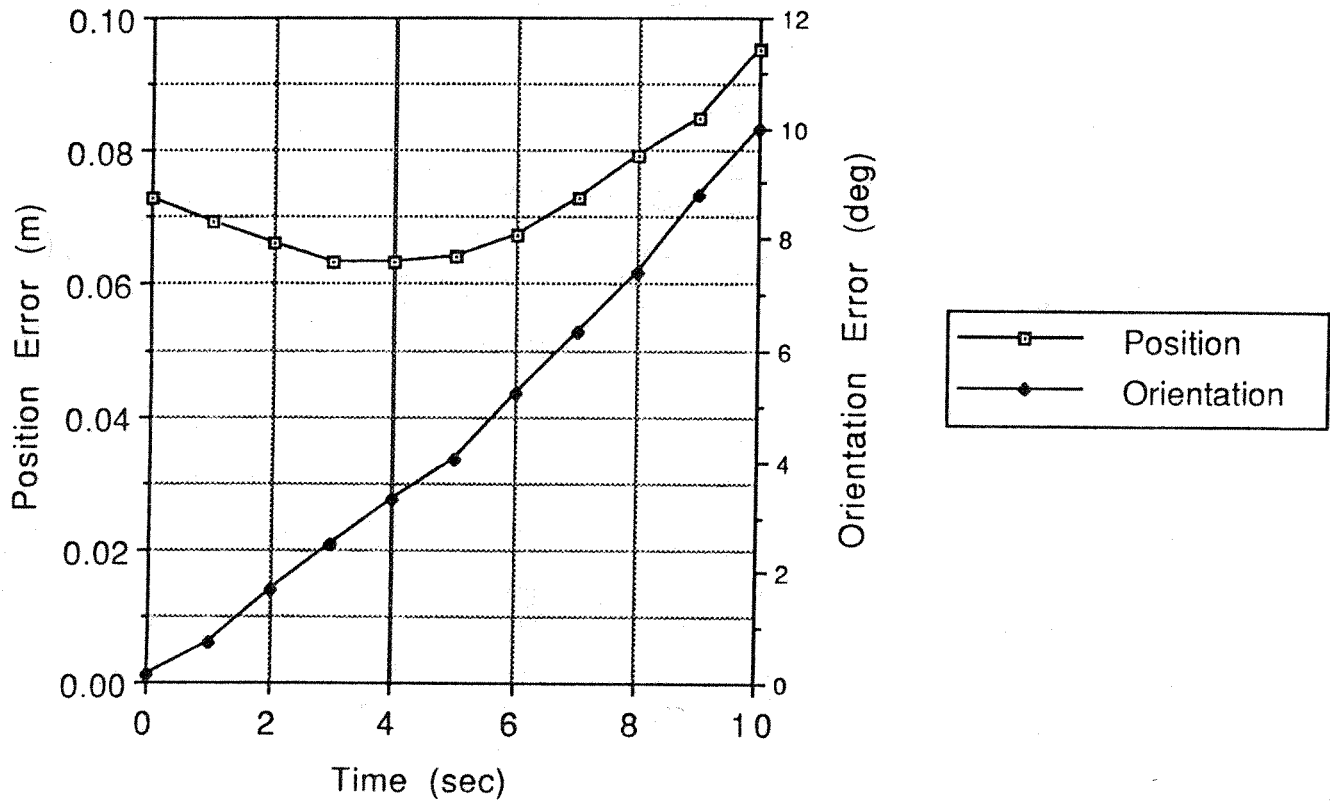


Figure 12c
Simplified Forward Model Error
VES Translation/Rotation Simulation



REPORT DOCUMENTATION PAGE

Form Approved
OMB No. 0704-0188

Public reporting burden for this collection of information is estimated to average 1 hour per response, including the time for reviewing instructions, searching existing data sources, gathering and maintaining the data needed, and completing and reviewing the collection of information. Send comments regarding this burden estimate or any other aspect of this collection of information, including suggestions for reducing this burden, to Washington Headquarters Services, Directorate for Information Operations and Reports, 1215 Jefferson Davis Highway, Suite 1204, Arlington, VA 22202-4302, and to the Office of Management and Budget, Paperwork Reduction Project (0704-0188), Washington, DC 20503.

1. AGENCY USE ONLY (Leave blank)		2. REPORT DATE March 1992	3. REPORT TYPE AND DATES COVERED Technical Memorandum	
4. TITLE AND SUBTITLE Kinematics of an In-Parallel Actuated Manipulator Based on the Stewart Platform Mechanism			5. FUNDING NUMBERS 595-11-22	
6. AUTHOR(S) Robert L. Williams II				
7. PERFORMING ORGANIZATION NAME(S) AND ADDRESS(ES) NASA Langley Research Center Hampton, Virginia 23665-5225			8. PERFORMING ORGANIZATION REPORT NUMBER	
9. SPONSORING / MONITORING AGENCY NAME(S) AND ADDRESS(ES) National Aeronautics and Space Administration Washington, DC 20546-0001			10. SPONSORING / MONITORING AGENCY REPORT NUMBER NASA TM-107585	
11. SUPPLEMENTARY NOTES				
12a. DISTRIBUTION / AVAILABILITY STATEMENT Unclassified - Unlimited Subject Category 63			12b. DISTRIBUTION CODE	
13. ABSTRACT (Maximum 200 words) This paper presents kinematic equations and solutions for an in-parallel actuated robotic mechanism based on Stewart's platform. These equations are required for inverse position and resolved rate (inverse velocity) platform control. NASA Langley has a Vehicle Emulator System (VES) platform designed by MIT which is based on Stewart's platform. The inverse position solution is straight-forward and computationally inexpensive. Given the desired position and orientation of the moving platform with respect to the base, the lengths of the prismatic leg actuators are calculated. The forward position solution is more complicated and theoretically has 16 solutions. The position and orientation of the moving platform with respect to the base is calculated given the leg actuator lengths. Two methods are pursued in this paper to solve this problem. The resolved rate (inverse velocity) solution is derived. Given the desired Cartesian velocity of the end-effector, the required leg actuator rates are calculated. The Newton-Raphson Jacobian matrix resulting from the second forward position kinematics solution is a modified inverse Jacobian matrix. Examples and simulations are given for the VES.				
14. SUBJECT TERMS Stewart Platform, Kinematics, Manipulator, Parallel manipulator, Forward Transform, in-Parallel Actuator			15. NUMBER OF PAGES 53	
			16. PRICE CODE A04	
17. SECURITY CLASSIFICATION OF REPORT Unclassified	18. SECURITY CLASSIFICATION OF THIS PAGE Unclassified	19. SECURITY CLASSIFICATION OF ABSTRACT Unclassified	20. LIMITATION OF ABSTRACT Unlimited	